

# **Understanding changes in precipitation with climate change over wet and dry land**

by

Sarah Weidman

Submitted to the Department of Earth, Atmospheric and Planetary  
Science

in partial fulfillment of the requirements for the degree of

Bachelor of Science in Earth, Atmospheric and Planetary Science

at the

MASSACHUSETTS INSTITUTE OF TECHNOLOGY

June 2021

© Massachusetts Institute of Technology 2021. All rights reserved.

Author .....  
.....

Department of Earth, Atmospheric and Planetary Science  
May 14, 2021

Certified by .....  
.....

Paul O'Gorman  
Professor  
Thesis Supervisor

Accepted by .....  
.....

Richard Binzel  
Chairman, Committee on Undergraduate Program

# **Understanding changes in precipitation with climate change over wet and dry land**

by

Sarah Weidman

Submitted to the Department of Earth, Atmospheric and Planetary Science  
on May 14, 2021, in partial fulfillment of the  
requirements for the degree of  
Bachelor of Science in Earth, Atmsopheric and Planetary Science

## **Abstract**

Observed precipitation increased moderately in both wet and dry regions over the past 60 years, contradicting the wet-gets-wetter, dry-gets-drier (WWDD) mechanism. This study uses the perturbation atmospheric energy budget to understand the projected increase in precipitation over dry and wet land with climate change. Using global climate model output, the change in each term in the perturbation energy budget was calculated as a regional average over wet and dry tropical land. Increases in precipitation over wet and dry tropical land are primarily driven by increases in radiative loss, which are moderated by increases in sensible heat flux. Although the dry static energy flux divergence has a strong spatial pattern, cancellation between the horizontal and vertical advection terms, as well as cancellation between the dynamic and thermodynamic components of vertical advection, result in relatively small contributions from the dry static energy flux divergence towards the change in precipitation in the regional average. Only when wet and dry regions are allowed to change seasonally is WWDD given, suggesting that the movement of wet and dry regions is a significant factor in opposing the WWDD mechanism over land.

Thesis Supervisor: Paul O’Gorman  
Title: Professor

## Acknowledgments

GFDL-CM3 climate model output was retrieved from the GFDL node at <https://nomads.gfdl.noaa.gov/>. Code to compute vertical velocity in hybrid sigma coordinates was generously provided by Ziwei Li. Computing resources were provided by the EAPS cluster.

I would like to thank Paul O’Gorman for invaluable advice and mentorship throughout the course of this project. Thank you also to Jane Abbott for communication instruction, and to the EAPS department for being a welcoming community.

I also thank my family and roommates for their patience and support throughout this thesis-writing process, and to Howard Shore and *The Lord of the Rings* soundtrack for its incessant motivation.

*... its secrecy in springs, and latent humidity, revealed by rhabdomantic or hygrometric instruments and exemplified by the hole in the wall at Ashtown gate, saturation of air, distillation of dew: the simplicity of its composition, two constituent parts of hydrogen with one constituent part of oxygen: its healing virtues: its buoyancy in the waters of the Dead Sea: its preserving penetrativeness in runnels, gullies, inadequate dams, leaks on shipboard: its properties for cleansing, quenching thirst and fire, nourishing vegetation: its infallibility as paradigm and paragon: its metamorphoses as vapour, mist, cloud, rain, sleet, snow, hail...*

James Joyce, *Ulysses*

# Contents

<b>1</b>	<b>Introduction</b>	<b>8</b>
<b>2</b>	<b>Methods</b>	<b>13</b>
2.1	Model and data . . . . .	13
2.2	The perturbation atmospheric energy budget equation . . . . .	14
2.3	Defining terms in the energy budget . . . . .	16
2.4	Selecting wet and dry regions . . . . .	19
<b>3</b>	<b>Regionally-averaged energy budget</b>	<b>21</b>
3.1	The regionally-averaged energy budget over wet and dry tropical land	21
3.2	Sensible heat flux . . . . .	24
3.3	Dynamic and thermodynamic advective components . . . . .	26
3.4	Weakening circulation . . . . .	28
3.5	Cancellation of vertical and horizontal advection . . . . .	31
<b>4</b>	<b>Further interpretations of the tropical energy budget</b>	<b>34</b>
4.1	Shifting wet and dry regions . . . . .	34
4.2	Precipitation - Evaporation . . . . .	38
<b>5</b>	<b>Conclusions</b>	<b>40</b>
<b>A</b>	<b>Calculating advection terms using hybrid sigma coordinates</b>	<b>42</b>
<b>B</b>	<b>Extensions to the midlatitudes</b>	<b>45</b>



# List of Figures

1-1	Change in average annual precipitation . . . . .	9
1-2	Global atmospheric energy budget . . . . .	11
2-1	Maps of terms in the energy budget . . . . .	16
2-2	Wet and dry tropical land regions . . . . .	19
3-1	Energy budget over wet and dry tropical land . . . . .	22
3-2	Dynamic and thermodynamic components of vertical advection . . . .	27
3-3	Structure of vertical velocity . . . . .	30
3-4	Cancellation of vertical and horizontal advection . . . . .	32
4-1	Change in precipitation in shifted regions . . . . .	35
4-2	Energy budget over seasonally-shifted regions . . . . .	37
4-3	Change in $P - E$ . . . . .	38
B-1	Maps of energy budget terms including the midlatitudes . . . . .	46
B-2	Wet and dry land regions . . . . .	47
B-3	Energy budget over wet and dry land including the midlatitudes . . .	48
B-4	Dynamic and thermodynamic components in the midlatitudes . . . .	49
B-5	(P-E) in the midlatitudes . . . . .	50

# Chapter 1

## Introduction

Climate change projections consistently predict an increase in global temperatures and concentration of atmospheric CO<sub>2</sub> in the coming century. Increasing temperatures and CO<sub>2</sub> concentrations will affect the climatological patterns of precipitation, which are tightly tied to water availability, ecosystem health, and human habitability. Changes in precipitation due to climate change are expected to both decrease available freshwater resources for dry subtropical regions and increase severe flooding in coastal and river basin regions (Pachauri & Meyer, 2014). The spatial pattern of precipitation changes due to climate change is nonuniform, and any changes we see over land will profoundly affect the people living there (Figure 1-1).

Many prior studies have investigated theories behind the physical mechanisms driving changes in precipitation, but the complexity of the climate system results in uncertainty around the strength and interplay of these mechanisms in different regions. One mechanism that has been used to explain large-scale changes in ocean precipitation patterns is the enhancement of climatological precipitation minus evaporation ( $P - E$ ), dubbed the “wet-get-wetter, dry-get-drier” (WWDD) mechanism (Held & Soden, 2006; Chou & Neelin, 2004). This mechanism follows the Clausius-Clapeyron relation, which is a thermodynamic relationship that implies an increase in specific humidity of the air by about 7% per °C of warming. According to the WWDD mechanism, an increase in atmospheric water vapor in a warming climate with approximately constant relative humidity will result in an increase in moisture

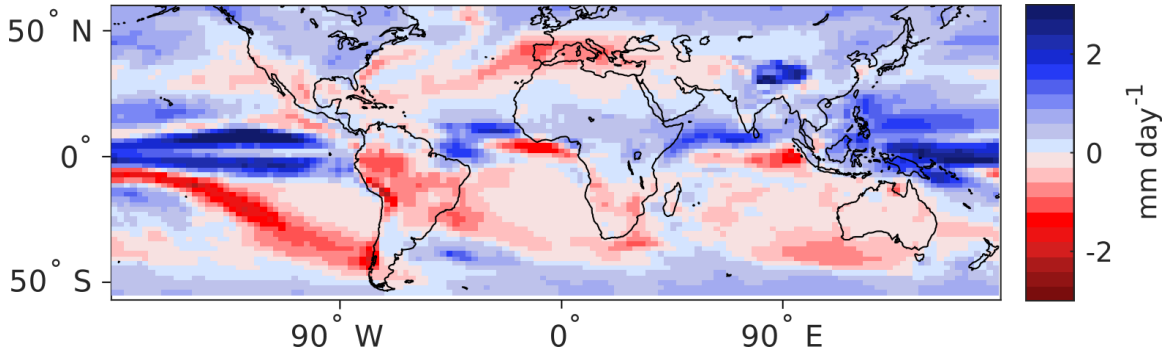


Figure 1-1: Change in average annual precipitation between (2081-2100) and (1980-1999) in  $\text{mm day}^{-1}$ . Increases in precipitation are in blue and decreases are in red. This and all future figures use GFDL-CM3 model output with the RCP 8.5 emissions scenario for simulating the (2081-2100) period.

transport: regions with already high moisture convergence (often wet tropical regions) will see a further increase in precipitation, while regions with moisture divergence (often dry subtropical regions) will get drier. The WWDD mechanism is most relevant over oceans, where changes in the surface relative humidity are small (compared to potentially large changes in surface moistness over dry land regions), and when averaged over full latitudinal zones (Held & Soden, 2006). This simple mechanism breaks down at regional scales due to dynamical changes (Chadwick et al., 2013; Roderick et al., 2014).

The WWDD mechanism does not seem to dominate changes in precipitation over land in either observational data or model simulations, and it is crucial that we understand the changes over the habited parts of our planet. Observations of recent changes in precipitation over land show increases in precipitation in wet regions, but large variability in changes in precipitation over dry regions with no clear trend in aggregate annual precipitation changes (Greve et al., 2014; Greve & Seneviratne, 2015). However, these observed studies were performed at a gridpoint basis, rather than over a larger scale as required by the WWDD mechanism (Chadwick et al., 2013). Donat et al. (2016) tried to reduce the noise introduced by large internal variability at the gridpoint-level by splitting both observational data and model output into globally wet and dry regions based on total annual precipitation. In observations of annual precipitation from 1950-2010, they found a statistically significant increase in

precipitation of 1-2% per decade in dry land regions, but no significant trend in wet land regions. Observations of precipitation have large gaps over the Sahara and the Amazon, but similar trends in changes in precipitation were replicated across wet and dry land in global climate models. This is contradicts what is expected by the WWDD mechanism and is worth investigating why.

Several studies have hypothesized reasons for why the WWDD mechanism does not hold over land, but there is as-yet no simple mechanism that explains the patterns we do observe. For one, the WWDD mechanism assumes that relative humidity remains approximately constant with climate change. Chadwick et al. (2013) proposed that over land, relative humidity decreases and works to oppose the WWDD mechanism. Byrne and O’Gorman (2015) used the atmospheric moisture budget to expand this argument by determining that fractional changes in relative humidity and horizontal temperature gradients are important in explaining the pattern of changes in  $P - E$  over land. Their new scaling better represents regions of both increased and decreased  $P - E$  over land, but it does not take into account circulation changes which could be especially important in the tropics and subtropics. Circulation changes could play a large role in increasing precipitation in dry regions: if changes in circulation shifts a historically wet region into a dry region, the average precipitation would inherently increase in that defined region (Polson & Hegerl, 2017).

The atmospheric water vapor budget has been useful in determining changes in  $P - E$  over ocean (Seager et al., 2010; Held & Soden, 2006; Trenberth & Guillemot, 1995), but an energetic approach could be a simpler way to explain the mechanisms involved for the precipitation on its own (Pierrehumbert, 2002; Allen & Ingram, 2002; O’Gorman et al., 2012; Muller & O’Gorman, 2011), especially when considering the complexity of causes of change in  $P - E$  over land which involve subtle changes in gradients of relative humidity and temperature (Byrne & O’Gorman, 2015). Using the atmospheric energy budget, global changes in precipitation can be explained by changes in radiative loss and surface sensible heat flux at a global scale:

$$L_c \delta P = \delta Q_{rad} - \delta SH \quad (1.1)$$

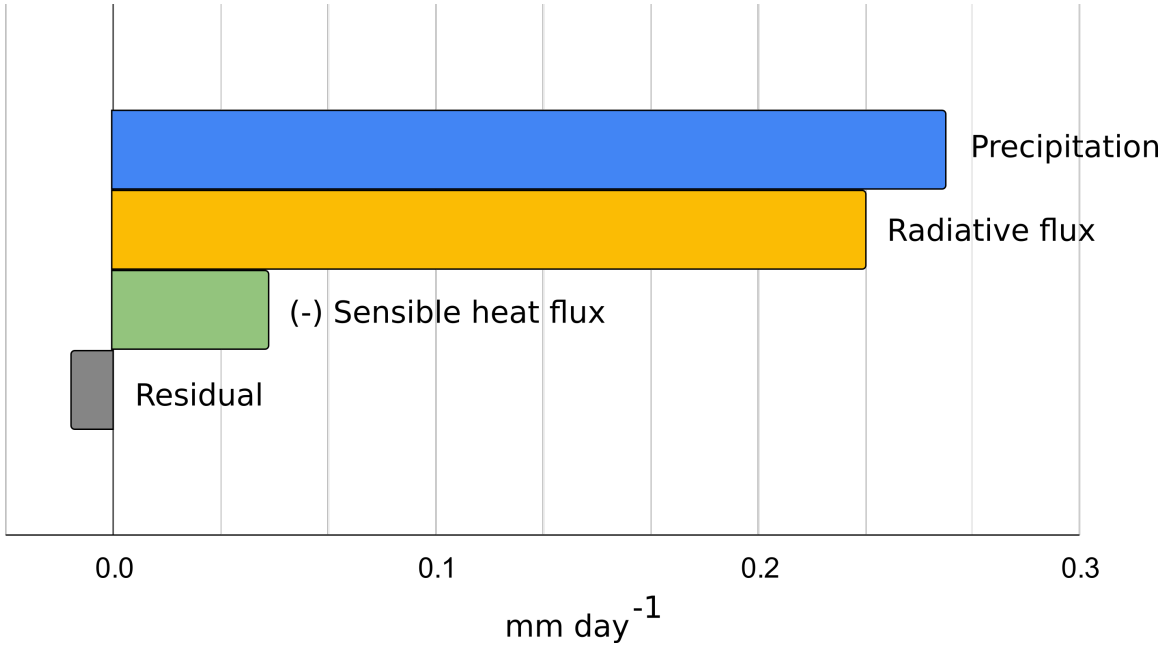


Figure 1-2: Change in magnitude and sign of each term in the atmospheric energy budget between (1980-1999) and (2081-2100) expressed in  $\text{mm day}^{-1}$ , averaged over the full globe. The residual is calculated as the difference between precipitation and the sum of radiative and sensible heat flux.

where  $P$  is annual precipitation,  $Q_{rad}$  is net radiative loss,  $SH$  is surface sensible heat flux,  $L_c$  is the latent heat of condensation of water, and  $\delta$  refers to the change from a historical to future climate period. The global energy budget is shown in Figure 1-2, where each term is the difference between a future climate period (2081-2100) and a historical period (1980-1999), averaged over all land and ocean regions. Globally we expect to see an increase in precipitation; energetically, this increase in precipitation is balanced by an increase in radiative loss and negative sensible heat flux. Muller and O’Gorman (2011) demonstrated that the atmospheric energy budget can also describe local changes in precipitation by including horizontal energy transport through the dry static energy flux divergence. We expect the relative balances between terms in the energy budget to differ over land and over wet and dry regions, and those differences can inform which physical mechanisms most influence changes in precipitation in each type of region.

Following Donat et al. (2016); Liu and Allan (2013), wet and dry regions over land can be chosen by considering regions with the highest and lowest average annual

precipitation. We acknowledge that this does not fully characterize the wetness or dryness of a land region, but it is a reasonable approach for the tropical land regions that are the focus of this study. Over the tropics, where horizontal eddy fluxes of dry static energy are small due to weak horizontal temperature gradients, an energetic approach can cleanly illustrate the mechanisms involved in setting the pattern of precipitation changes over land. Observationally, it is difficult to measure evaporation, though we can clearly measure the amount of precipitation using rain gauges, further motivating the use of an energetic approach that can help interpret changes in precipitation rather than changes in precipitation minus evaporation.

In this thesis, the perturbation atmospheric energy budget equation as derived by Muller and O’Gorman (2011) is used to explain patterns of changes in precipitation averaged over dry and wet land regions. Global climate model output is used to look in depth at each term in the energy budget equation and determine which mechanisms are most important in setting changes in precipitation patterns over land. Section 2 contains general methods and describes the atmospheric energy budget equation used for this study. Analyses of the interplay between terms in the regionally-averaged energy budget in wet and dry land regions are described in section 3. Section 4 examines how the selection of wet and dry regions, as well as the use of precipitation rather than  $P - E$ , affects results. The bulk of results are constrained to the tropics to simplify the dynamics, but analyses are extended to changes in precipitation over the midlatitudes in Appendix B. A summary and discussion of the study can be found in section 5.

# Chapter 2

## Methods

### 2.1 Model and data

Global climate model data was used to examine changes in terms of the perturbation atmospheric energy budget over wet and dry land regions with climate change. Analyses of the energy budget were performed using one ensemble member of the NOAA GFDL-CM3 global climate model (Donner et al., 2011; Delworth et al., 2006). For this study, one model was used for simplicity and because climatologically wet and dry regions change between models, clouding any interplay or cancellation between terms of the energy budget. Climate change was assessed by comparing model output from a simulation of historical climate and a simulation of future climate with some amount of projected anthropogenic forcing. The climate change scenario used for this project was the Representative Concentration Pathways (RCP) 8.5 forcing scenario as defined for CMIP5 (Moss et al., 2008). RCP 8.5 is the forcing scenario with the largest amount of radiative forcing by 2100:  $8.5 \text{ W m}^{-2}$ . Although RCP 8.5 may not be the most realistic projection—there is much uncertainty around which pathway will be observed by the end of the century—the strongest forcing level can best illuminate the signal of changes in precipitation and other variables. Land regions were selected as all regions in which the land fraction was larger than 25% following the threshold of blended land/sea boundaries in the HADCRUT observations (Morice et al., 2021).

Change in precipitation and other variables were determined as the difference in the average annual mean over 2081-2100 (the “RCP” period) and over 1980-1999 (the “historical” period). In some situations, seasonality was expected to have an impact on results, so changes were computed as the difference between Jan-Mar, Apr-Jun, Jul-Sep, Oct-Dec means over the same 20 year periods. Since the statistics of interest were annual average changes over time, using monthly data was sufficient for most variables. However, for the horizontal and vertical advection terms, information about the movement of eddies can be lost when averaging over months or days. For these terms, 6-hourly data was used. The 6-hourly data also increased the number of vertical levels of the data by using the direct (non-interpolated) model output in hybrid sigma coordinates. This further improved the accuracy of the advection terms since both are computed by integrating over the vertical extent of the atmosphere. 6-hourly data with 48 vertical levels were used for specific humidity, temperature, eastward wind, northward wind, and surface pressure (one vertical level). Vertical velocity was computed from these variables using the continuity equation as described in Simmons and Burridge (1981) Equation 2.5. Monthly data were sufficient for all other variables. The horizontal grid spacing for all variables is  $2^\circ$  latitude x  $2.5^\circ$  longitude.

Climate model output for energy flux terms are in  $\text{W m}^{-2}$ . All analyses have been converted into equivalent precipitation units of  $\text{mm day}^{-1}$ . The following conversion was used to convert between these units:

$$\frac{86400 \text{ seconds}}{\text{day}} \frac{1}{L_c} \frac{1000 \text{ mm}}{\text{m}} \frac{1}{\rho_{\text{water}}} \approx \frac{1}{29} \text{ mm day}^{-1} \text{ W}^{-1} \text{ m}^2 \quad (2.1)$$

## 2.2 The perturbation atmospheric energy budget equation

Muller and O’Gorman (2011) showed that the atmospheric energy budget (Equation 1.1) holds for regional changes when including energy transport terms:

$$L_c \delta P = \delta Q_{rad} - \delta SH + \delta H \quad (2.2)$$

Where  $P$  is average precipitation,  $Q_{rad}$  is radiative loss,  $SH$  is surface sensible heat flux,  $H$  is the dry static energy flux divergence, and  $L_c$  is the latent heat of condensation of water (neglecting the latent heat of fusion, and thus melting and freezing). The physical meaning of each term will be defined in the following section. The dry static energy flux divergence can be written as:

$$\delta H = \delta \int_0^{p_s} (\mathbf{u} \cdot \nabla s) \frac{dp}{g} \quad (2.3)$$

Where  $\mathbf{u}$  is the 3-dimensional wind vector,  $p$  is pressure,  $p_s$  is surface pressure,  $s$  is the dry static energy  $s = c_p T + gz$ ,  $T$  is temperature,  $z$  is geopotential height above the reference geode in meters,  $c_p$  is the heat capacity of air and  $g$  is gravity. This term is integrated over the vertical extent of the atmosphere. The dry static energy flux divergence can be split into horizontal and vertical advective components as below:

$$\delta H_z = \delta \int_0^{p_s} \left( \omega \frac{\partial s}{\partial p} \right) \frac{dp}{g} \quad (2.4)$$

$$\delta H_{x,y} = \delta \int_0^{p_s} (\mathbf{u}_H \cdot \nabla_H s) \frac{dp}{g} \quad (2.5)$$

Equation 2.4 is the vertical advective term with  $\omega$  as the vertical velocity in pressure coordinates. Equation 2.5 is the horizontal advective term with  $\mathbf{u}_H$  as the horizontal wind vector, which includes  $u$  and  $v$  as zonal and meridional wind, respectively, and  $\nabla_H$  as the horizontal gradient in the  $x$  and  $y$  directions. Thus, our final perturbation atmospheric energy budget equation in spherical coordinates is:

$$L_c \delta P = \delta Q_{rad} - \delta SH + \delta \int_0^{p_s} \left( \omega \frac{\partial s}{\partial p} \right) \frac{dp}{g} + \delta \int_0^{p_s} \left( \frac{u}{a \cos(\phi)} \frac{\partial s}{\partial \lambda} + \frac{v}{a} \frac{\partial s}{\partial \phi} \right) \frac{dp}{g} \quad (2.6)$$

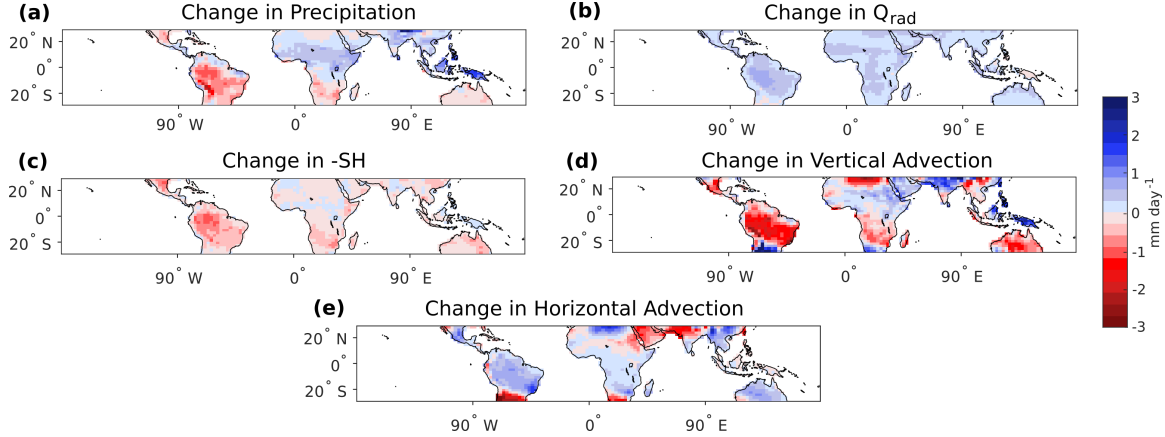


Figure 2-1: Change in each term of the energy budget from (1980-1999) to (2081-2100) in  $\text{mm day}^{-1}$ , evaluated at each gridpoint. On a large scale, change in precipitation (a) should be approximately balanced by changes in radiative flux divergence (b), sensible heat flux (c), and the vertical (d) and horizontal (e) components of dry static energy flux divergence.

where  $a$  is the radius of the Earth,  $\phi$  is latitude and  $\lambda$  is longitude. The advection terms are integrated using 6-hourly data, and the time mean is taken over the fully integrated term. The full equations used with 6-hourly data in hybrid sigma coordinates are shown in Appendix A.

## 2.3 Defining terms in the energy budget

The atmospheric energy budget equation is useful because total energy is conserved throughout the global atmosphere, so in a perfect model, changes in precipitation will be completely balanced by the sum of the terms on the right side of Equation 2.6. Precipitation appears in the energy budget because of latent heating: the energy associated with a change of phase, such as condensation during precipitating events (Peixoto & Oort, 1992). The pattern of change in precipitation over tropical land is plotted in Figure 2-1a. Maps of each term in the energy budget over land and ocean and extending into midlatitudes are plotted in Figure B-1.

The radiative loss term (sometimes referred to as  $Q_{rad}$  or the radiative flux divergence) is the difference between net radiative flux at the top of the atmosphere and net radiative flux at the surface. Incoming solar radiation is zonally symmetric

depending on the angle at which sunlight strikes the earth. Outgoing longwave radiation is emitted from the atmosphere and the surface of the earth. Complexity in radiative flux arises from clouds, which absorb, emit, and reflect energy depending on the wavelength of the associated light and properties of the cloud particles (Peixoto & Oort, 1992). As the concentration of CO<sub>2</sub> increases in the atmosphere, more outgoing radiation is absorbed by the atmosphere instead of being released to space, and some of that energy is emitted back towards the surface, increasing surface temperatures (Marshall & Plumb, 2007). We expect to see an increase in radiative loss over time, but not necessarily a difference between wet and dry regions. Figure 2-1b displays this nearly uniform increase in radiative loss over tropical land. Global precipitation is sometimes taken to be radiatively constrained, where excess energy driven by increased radiative loss is converted to latent heat (and precipitation) (Allen & Ingram, 2002), but this argument is complicated by changes in sensible heat flux (Schneider et al., 2010).

The surface sensible heat flux term is the dry counterpart to latent heat flux; it is the conductive heat flux at the surface without a corresponding phase change. Heat is transferred from the Earth's surface to the lowest layer of the atmosphere or from the atmosphere to the surface due to a difference in temperature between the surface and the air above (Peixoto & Oort, 1992). Surface sensible heat can depend on many aspects of the land surface, including surface air and ground temperature, surface winds, and vegetation characteristics (Pierrehumbert, 2010). These quantities are difficult to measure and model accurately over land since the land surface is so heterogeneous (McColl et al., 2019). Positive changes in surface sensible heat flux contributes to a negative change in precipitation, so the negative change in sensible heat is plotted in Figure 2-1c. With climate change, sensible heat flux increases over land but decreases over ocean (Figure B-1c); this effect is discussed more deeply in section 3.2.

The flux of dry static energy describes the transport of atmospheric energy by the circulation (winds). The dry static energy flux divergence is where most of the local differences in the atmospheric energy budget appear. As shown in Equations 2.4

and 2.5, changes in dry static energy flux divergence can be separated into vertical and horizontal advective components. The vertical component is associated with changes in vertical velocity and vertical structure of the atmosphere. The pattern of changes in vertical advection is large over land and ocean (Figure 2-1d). The vertical advection term can be further split into two components: a dynamic component that captures changes in vertical velocity, and a thermodynamic component that captures changes in temperature structure:

$$\delta H_{z,dyn} = \int_0^{p_s} \left( \delta \omega \cdot \frac{\partial \bar{s}}{\partial p} \right) \frac{dp}{g} \quad (2.7)$$

$$\delta H_{z,therm} = \int_0^{p_s} \left( \bar{\omega} \cdot \delta \frac{\partial s}{\partial p} \right) \frac{dp}{g} \quad (2.8)$$

following the decomposition in Muller and O’Gorman (2011). Overbars signify a time mean over the historical and climate change period. The dynamic component of vertical advection (Equation 2.7) describes changes in vertical velocity, which are associated with dynamical changes in circulation, such as changes in current large-scale circulation patterns (which would include the movement of climatologically wet or dry regions with time) or changes in tropopause height. The thermodynamic component is associated with changes in mean dry static stability (Equation 2.8) and thus changes in temperature structure; its dependence on temperature gives it similar behavior to the simple thermodynamic scaling associated with the WWDD mechanism.

The horizontal advective component of dry static energy flux divergence describes changes in horizontal gradients of dry static energy and horizontal winds. In most regions, horizontal advection opposes vertical advection but with a weaker magnitude, resulting in some amount of cancellation between the advective terms (Figure 2-1e). In this study, the eddy geopotential component of horizontal advection was neglected due to issues with noise in the model output from orography. Instead, the geopotential component of horizontal advection was calculated using monthly data. In the annual mean, the eddy geopotential component is expected to be insignificant, making this

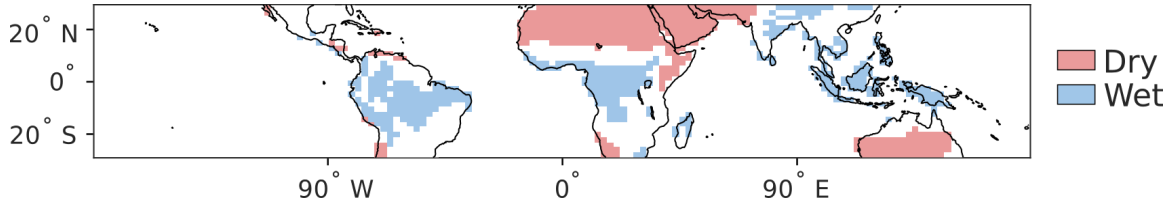


Figure 2-2: Wet (blue) and dry (red) regions based on the gridpoints with the 30% highest (wet) and lowest (dry) average annual precipitation from 1980-1999 and 2081-2100, and restricted to land between 30 °S and 30 °N.

a reasonable approximation.

## 2.4 Selecting wet and dry regions

Wet and dry regions were selected by determining the average annual precipitation over both (1980-1999) and (2081-2100) at each gridpoint. Gridpoints were then sorted into an index of least to most average annual precipitation (see Donat et al. (2016)). The 30% of gridpoints in the region of interest (i.e. tropical land, land between 60 °S and 60 °N, or tropical ocean) with the highest average annual precipitation were classified as wet regions, and the lowest 30% as dry regions. Tropical regions were classified as regions between 30 °S to 30 °N. Wet and dry tropical land regions are plotted in Figure 2-2, with a similar plot of wet and dry land between 60 °S and 60 °N in Figure B-2. The wet and dry tropical land regions are similar to the “arid” and “humid” regions as defined by UNESCO, though 30% is likely too narrow to capture arid regions in Mexico and humid regions in SE Asia (Zarch et al., 2015).

Since dry and wet regions are expected to shift slightly over time, a small shift of wetter conditions into a historically dry region could significantly skew results towards the wetter conditions. Using the full 40-year period reduces the likelihood of experiencing biases from the “regression to the mean” phenomenon which would appear if dry and wet indices were selected from the historical period only (see addendum of Donat et al. (2016)). Polson and Hegerl (2017) examined the validity of the WWDD phenomenon over land with a different methodology for selecting wet and dry regions. Their analyses suggest that by allowing wet and dry regions to change over time and

over different seasons, there is a more robust WWDD pattern over land. This effect is discussed more deeply in section 4.1. All other analyses were performed with the fixed regions described above.

# Chapter 3

## The regionally-averaged perturbation atmospheric energy budget

### 3.1 The regionally-averaged energy budget over wet and dry tropical land

In order to observe patterns at a large scale and reduce the noise of internal variability at individual gridpoints, each term of the energy budget pictured in Figure 2-1 was spatially averaged over the wet and dry regions described in section 2.4. Regional averages of the energy budget over wet and dry tropical land regions (shown in Figure 2-2) and wet and dry tropical ocean regions (not pictured) are displayed in Figure 3-1. The residual term is calculated as the difference between the change in precipitation and the sum of terms on the right side of Equation 2.6. Similar spatially-averaged energy budgets for wet and dry land in the extratropics can be found in Figure B-3.

Precipitation increases in all regions, wet and dry. Donat et al. (2016) reports results over wet and dry land (all land north of 60° S) in %/K between (1951-1980) and (2070-2099), finding a multi-model mean increase in annual precipitation of 3 %/K over dry land and (nonsignificant) less than 1 %/K over wet land, seeming to contradict the paradigm of WWDD. Over the same latitudes and converted into %/K,

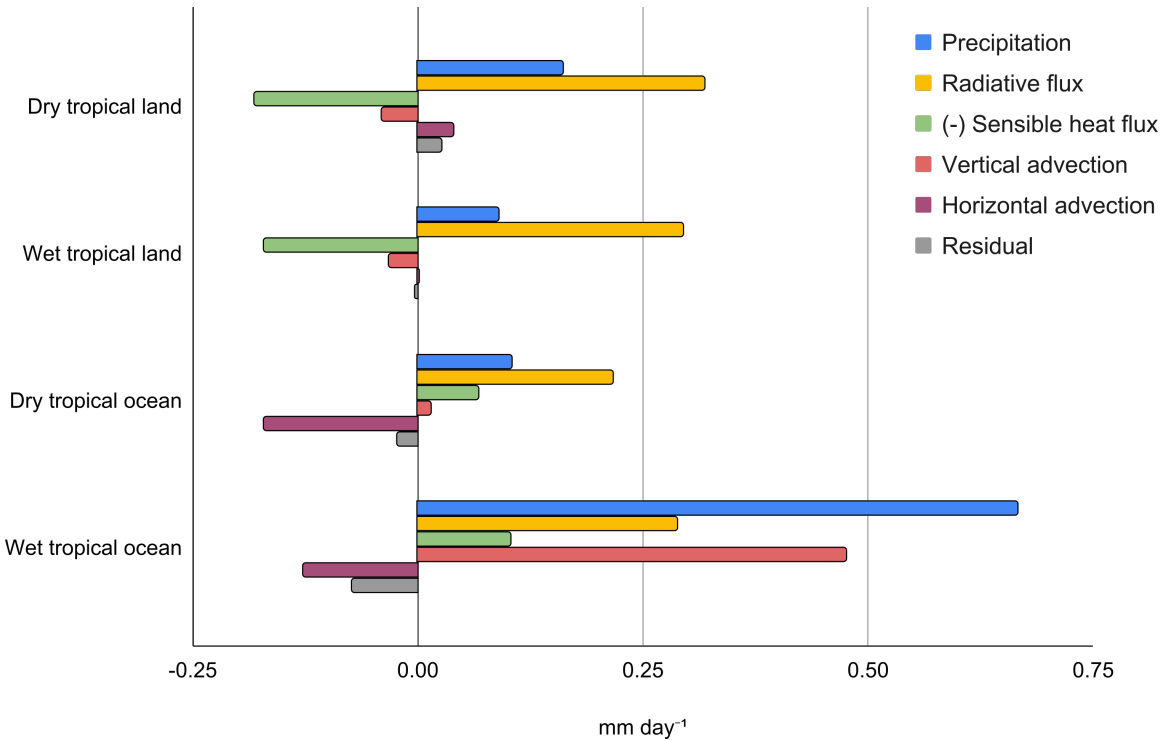


Figure 3-1: Regional averages of changes in each term of the energy budget in  $\text{mm day}^{-1}$ , as in Figure 2, but with spatial averages restricted to four regions: dry tropical land, wet tropical land, dry tropical ocean, and wet tropical ocean. Regions are constrained between  $30^{\circ}\text{S}$  and  $30^{\circ}\text{N}$ . Residual is calculated as the difference between precipitation and the sum of radiative loss, sensible heat flux, vertical advection, and horizontal advection for each region.

we found corresponding increases in precipitation of 2.3 %/K over dry land and 0.6 %/K over wet land between (1980-1999) and (2081-2100).

In all tropical regions, radiative loss strongly increases with climate change, contributing positively to the change in precipitation. Especially over land, an increase in energy loss from net radiation dominates, leading to an increase in precipitation. The radiative loss term is moderated over land by the sensible heat flux. Sensible heat flux contributes negatively towards a change in precipitation over both wet and dry land, corresponding to an increase in sensible heat flux. However, sensible heat flux is not strong enough to fully compensate for the increase in energy flux from radiative loss, resulting in an increase in precipitation in both wet and dry regions. Over the ocean, sensible heat flux has the opposite sign; sensible heat flux decreases in both wet and dry ocean regions (and globally), contributing, with radiative loss, to increases in precipitation. The difference between land and ocean sensible heat fluxes will be discussed in the following section.

Although the horizontal and vertical advection terms describe most of the spatial variation of change in precipitation in Figure 2-1a, these terms tend to play a smaller role when averaged over larger regions. In most cases, the change in horizontal and vertical advection terms have opposing signs, except in tropical wet land regions. Over land, their average contribution to change in precipitation is small; rather, the sign and magnitude of the change in precipitation in land regions seems to be almost entirely set by the balance of radiative and sensible heat fluxes, analogous to the global energy budget in Figure 1-2. However, in the tropical land case, sensible heat flux increases and opposes the increase in precipitation, which is the opposite sign to the global mean budget. Over tropical ocean regions (as in the global case), radiative and sensible heat fluxes both contribute towards an increase in precipitation. Here, the advective terms play a stronger role: vertical advection is a strongly positive feedback in wet regions while horizontal advection is negative in both wet and dry regions.

The cancellation of vertical and horizontal advection is more evident in Figure 2-1, where negative changes in vertical advection tend to correspond to increases in hori-

zontal advection and vice versa. In the regionally-averaged budget, this cancellation is most clear over dry tropical land (and over wet and dry land in Figure B-3), but does not seem to occur in the regional average over other tropical regions. This opposition and potential cancellation of vertical and horizontal advection are discussed in section 3.5.

## 3.2 Sensible heat flux

Of all the terms in the energy budget, sensible heat flux displays the biggest contrast between land and ocean regions. Sensible heat decreases over ocean regions (and in the global average), while it generally increases over land. The difference between land and ocean can be explained using the surface energy budget:

$$\delta R_{net} = \delta G + \delta SH + \delta LH \quad (3.1)$$

where  $R_{net}$  is the net radiation at the surface (related to  $Q_{rad}$ ),  $G$  is the ground heat flux,  $SH$  is the sensible heat flux, and  $LH$  is the latent heat flux.  $G$  is usually small compared to  $R_{net}$  and can be neglected here.

Increases in absorbed radiative energy due to climate change are not perfectly balanced by longwave radiation emissions at the surface. Thus, surface temperatures increase and there is an excess of energy that must be dissipated through either sensible or latent heat flux. Both surface fluxes are linearly related to differences between the ground (or the surface of the ocean) and the air just above the surface:

$$SH = k_{SH}(T_{sfc} - T_{air}) \quad (3.2)$$

$$LH = k_{LH}(p_{sat}(T_{sfc}) - h_{air} \cdot p_{sat}(T_{air})) \quad (3.3)$$

where  $k_{SH}$  and  $k_{LH}$  are different constants of proportionality, subscript  $sfc$  corresponds to the ground level, subscript  $air$  corresponds to the air just above the surface,  $p_{sat}$  is the saturation vapor pressure at the corresponding temperature, and  $h_{air}$  is the relative humidity of air just above the surface (Pierrehumbert, 2010). The

Clausius-Clapeyron relation states that saturation vapor pressure has an exponential dependence on temperature. Thus, as long as there is enough moisture available for the surface air to remain saturated, the latent heat flux will increase faster than the sensible heat flux with increased temperature. Moisture supplied by the ocean allows for latent heat to increase without limit, at least until very high temperatures result in a stably stratified boundary layer (Pierrehumbert, 2002). Over land, the latent heat flux can only increase until moisture availability dries up, at which point the extra energy shifts from latent to sensible heat: hence the increased sensible heat fluxes over land in the energy budget. As a result, Equation 3.3 is only valid over surfaces with adequate moisture, such as ocean, large lakes, glaciers, or sufficiently moist soil.

Examining the surface energy budget over land becomes even more complicated due to the heterogeneity of the surface. Soil moisture and vegetation (which release moisture into the air via evapotranspiration) can influence available moisture at the surface and shift the balance between latent and sensible heat flux (see the nonuniform sensible heat flux change over land in Figures 2-1c and B-1c). With climate change, vegetation may play an increasingly important role in the surface energy balance. With increased CO<sub>2</sub>, plants tend to close their stomata because of the relative ease of absorbing CO<sub>2</sub>, which reduces the amount of water vapor that can exit the leaves (Zarakas et al., 2020). Lower transpiration may then decrease moisture availability in already densely-vegetated regions, shifting the surface energy balance towards increased sensible heat flux. Over forested regions (our wet regions), we might expect to see a consistent increase in sensible heat flux, but this is not true, especially when considering the rain forests of South America and Indonesia. Kooperman et al. (2018) examines this zonal asymmetry of sensible heat flux. Complexity further arises when examining model output of surface variables, which are particularly difficult to parameterize in a climate model (Monteith, 1965).

The heterogeneity and complexity of sensible heat fluxes over land are nearly completely erased when looking at regional averages; the magnitude of sensible heat flux does not vary much across wet or dry land regions. This is a limitation of the

energetic approach, since not all wet and dry land surfaces have similar responses to climate change.

### 3.3 Dynamic and thermodynamic advective components

As discussed in section 2.3, the vertical advection term can be split into a dynamic component, which is associated with changes in circulation, and a thermodynamic component, which can be thought of as the “wet-gets-wetter, dry-gets-drier” mechanism in the energy budget. Figure 3-2a,b shows the spatial pattern of both components. The dynamic and thermodynamic component tend to work in opposite directions, though the magnitude of the dynamic component is larger than the thermodynamic term in some regions. The thermodynamic term is even weaker in the extratropics (Figure B-4). As a result, the dynamic term is most important in setting the sign of the full vertical advection term, though the thermodynamic term tends to mute its magnitude in the tropics.

Examining regional averages over wet and dry tropical regions further illustrates the opposition between the dynamic and thermodynamic components (Figure 3-2c). In all cases the dynamic component is positive in dry regions and negative in wet regions, while the thermodynamic component has an opposite contribution. Thus, the thermodynamic term enhances the current pattern of precipitation, contributing to increased precipitation in wet regions and decreased precipitation in dry regions. This WWDD mechanism is offset by the dynamic component from changes in circulation, which cancel out the WWDD signal enough to see an increase in precipitation in dry regions. Over land, the sum of the two components results in a small total vertical advection component. Thus, despite the strong pattern in the dynamic term of Figure 3-2a, the spatially-averaged contribution towards change in precipitation is nearly completely cancelled by the thermodynamic component. Over wet tropical ocean, the thermodynamic term dominates, enhancing the WWDD pattern.

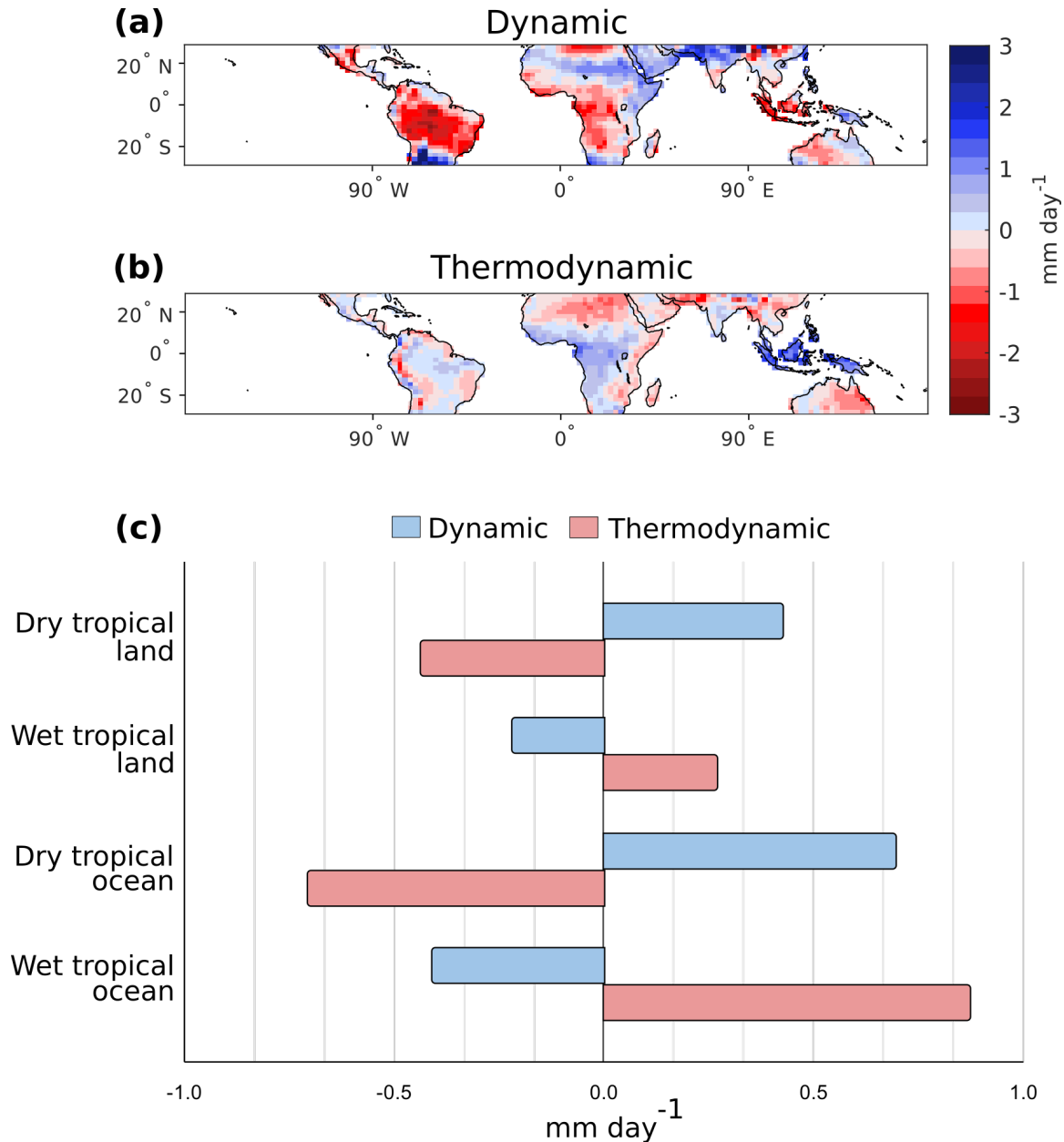


Figure 3-2: Dynamic (a) and thermodynamic (b) components of vertical advection, as defined in Section 2.3. Blue shading refers to a positive contribution towards increased precipitation, while red shading is a negative contribution. (c) displays the contributions of the dynamic (blue) and thermodynamic (red) components of vertical advection, spatially averaged over wet and dry tropical land (top two regions), and wet and dry tropical ocean (bottom two regions).

### 3.4 Weakening circulation

The dynamic component of vertical advection tells us that changes in circulation have a strong effect on setting the pattern of precipitation changes with climate change. Many previous studies have examined the effects of rising temperatures on changes in circulation; climate models project that tropical circulation patterns will decrease in strength with climate change (Held & Soden, 2006; Vecchi & Soden, 2007; Ma et al., 2012; He & Soden, 2015). Further, model simulations of climate change tend to show an upward shift of the tropopause, which would change the vertical extent of current circulation patterns (Singh & O’Gorman, 2012; Lorenz & DeWeaver, 2007). Examining the reasons for these changes in circulation is an active area of research and beyond the scope of this thesis, especially since climate models have been shown to overestimate the magnitude of weakening compared to observations (Sohn et al., 2016), but we examine whether our results align with previous work on circulation changes.

The strength and pattern of the tropical divergent circulation can be assessed using estimates of vertical velocity. A weakening circulation means that we should see a decrease in strength of ascending air in climatological ascent regions and descending air in descent regions. In this study, strength of ascent is measured by vertical velocity in pressure coordinates (negative in ascent regions and positive in descent regions), while ascent and descent regions are approximately “wet” and “dry” regions, respectively. Weakening of ascent and descent regions could refer to both 1) an overall weaker circulation that stays fixed over time or 2) a shift in location of climatological ascent or descent regions, since an ascent region moving into a descent region would “weaken” the circulation in that region by increasing the average upwards velocity. Further, by looking at changes in vertical velocity near the top of the troposphere, we can see whether the model simulates any changes in height of the tropopause.

We assess the strength of circulation by looking at changes in the magnitude of  $\omega$ . Since ascent and descent are often strongest at approximately 500 hPa (about 5 km in height), we use  $\omega$  at 500 hPa as an estimate of vertical velocity for the

full column. Conversely, changes in tropopause height (and other changes in the full vertical velocity profile) can be determined by looking at the changes in vertical structure of  $\delta\omega$ . We decompose the change in vertical velocity with climate change as:

$$\delta\omega_{magnitude} = \frac{\bar{\omega}}{\omega_{500}} \delta\omega_{500} \quad (3.4)$$

$$\delta\omega_{structure} = \delta \frac{\omega}{\omega_{500}} \bar{\omega}_{500} \quad (3.5)$$

where  $\omega_{500}$  is  $\omega$  at 500 hPa, overbars are an average over the two climate periods, and  $\delta$  is the change between the two periods. We then take regional averages of the full vertical profile of each component over wet and dry tropical land regions to examine changes in annual vertical velocity in ascent and descent regions (Figure 3-3). Since tropical circulation cells shift seasonally, similar analyses were performed for each season with corresponding seasonal wet and dry regions, but the results do not differ significantly from Figure 3-3 (not shown).

Over wet tropical land, the magnitude component of  $\delta\omega$  is positive in all seasons, which is consistent with a decrease in the strength of ascent in convective regions. In dry regions, there is a corresponding negative change in the magnitude of  $\omega$ , again consistent with a decrease in strength of descent. The strength of weakening when calculated as the percent change in the magnitude component of  $\delta\omega$  per degree K of warming is between 1-5 %/K in seasonal wet and dry tropical land regions, which aligns with estimates of weakening of 2-4 %/K as calculated by Vecchi and Soden (2007).

The structure component in Figure 3-3 describes at what height the largest changes in  $\omega$  tend to occur. Large values of the structure component around 800-900 hPa could relate to changes in boundary layer height or could be due to noise at the surface of the model. Since vertical velocity is close to 0 in the stratosphere, the change in sign of  $\delta\omega$  above 200-100 hPa corresponds to an increase in the height of the tropopause.

Figure 3-3 also displays the structure and magnitude components of vertical ve-

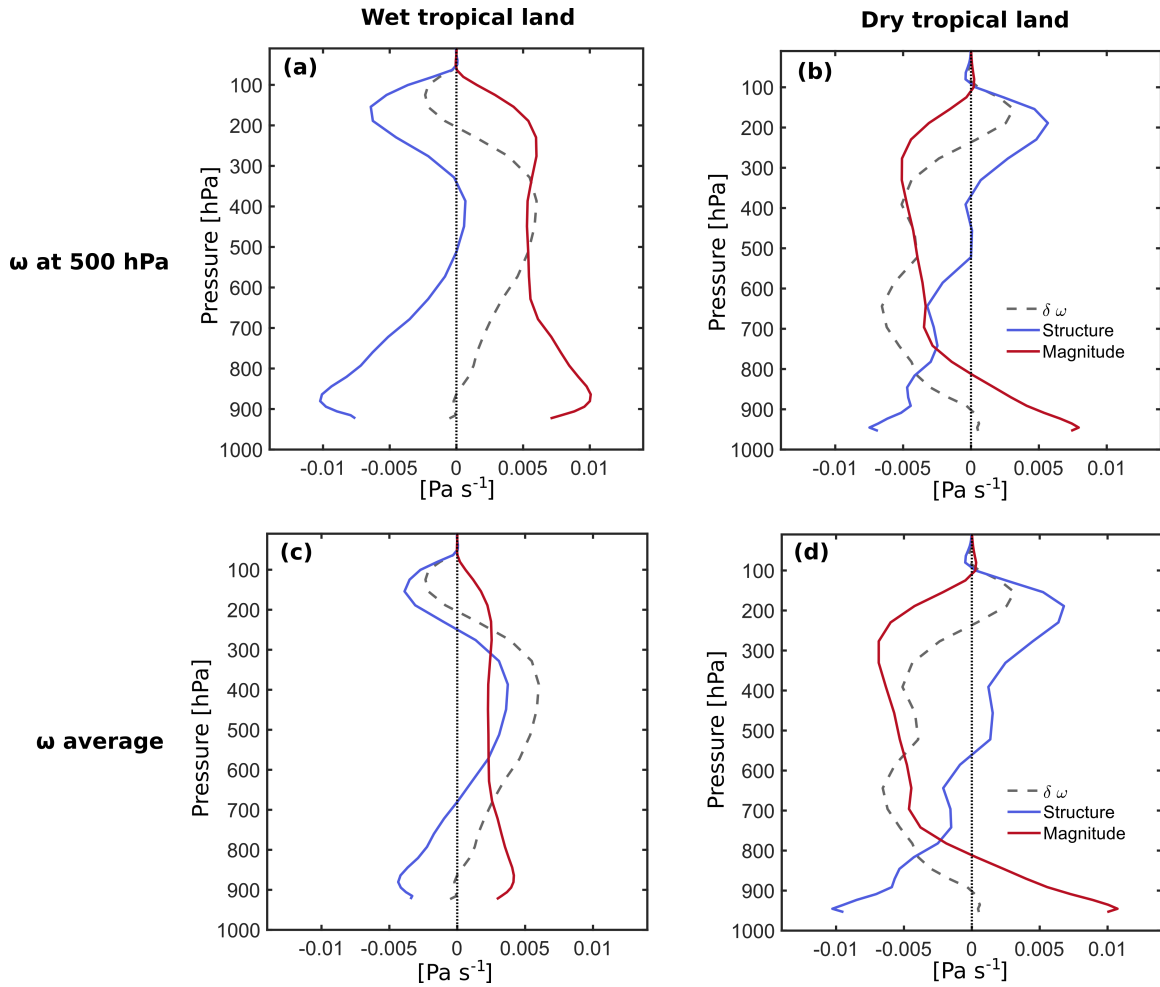


Figure 3-3: Change in vertical velocity between (1980-1999) and (2081-2100) (dashed grey) averaged over wet tropical land (left) and dry tropical land (right) regions. Change in vertical velocity is decomposed into changes in vertical structure (blue) and changes in magnitude (red). The magnitude component is taken as  $\omega$  at 500 hPa (top row) and the average of  $\omega$  over the full column (bottom).

locity, replacing  $\omega_{500}$  in Equations 3.4 and 3.5 with the average value of  $\omega$  over the full column. This choice helps reveal whether the choice of  $\omega$  at 500 hPa affects the results, since it is possible that the height at which the maximum ascent or descent occurs will change with climate change. The shape and sign of both components of average  $\omega$  are similar to  $\omega$  at 500 hPa with a slightly weaker change in magnitude in wet regions and stronger change in magnitude in dry regions. Most importantly, the sign of the magnitude component does not change when using  $\omega$  at 500 hPa or average  $\omega$ , suggesting that the model projects weakening across multiple vertical levels of the atmosphere.

This weakening result corresponds to the changes in the dynamic component of vertical advection discussed in section 3.3. Due to either an overall decrease in circulation strength or shifting of climatological ascent and descent regions, weakening circulation works against the WWDD mechanism of the thermodynamic component. Over tropical land regions, they nearly completely cancel out, leaving the vertical advection term very small in the spatial mean. The extent to which this result comes from weakening circulation or the movement of regions with time is discussed in section 4.1

### 3.5 Cancellation of vertical and horizontal advection

Regional averages of the vertical and horizontal advection terms tend to oppose each other in tropical regions (Figure 3-1), and nearly completely cancel in wet and dry regions that extend to the midlatitudes (Figure B-3). This cancellation is not simply a factor of taking regional averages; spatial maps of the advection terms show opposing signs at a gridpoint scale (Figures 2-1, B-1). Since horizontal advection is weak in the tropics, complete cancellation between the advection terms is more plausible at higher latitudes. Hoskins and Karoly (1981) describes a theory for why this cancellation occurs: for stationary waves, upward motion is associated with poleward motion (and downward with equatorward motion). With climate change and a decreased meridional temperature gradient, the vertical and horizontal advection

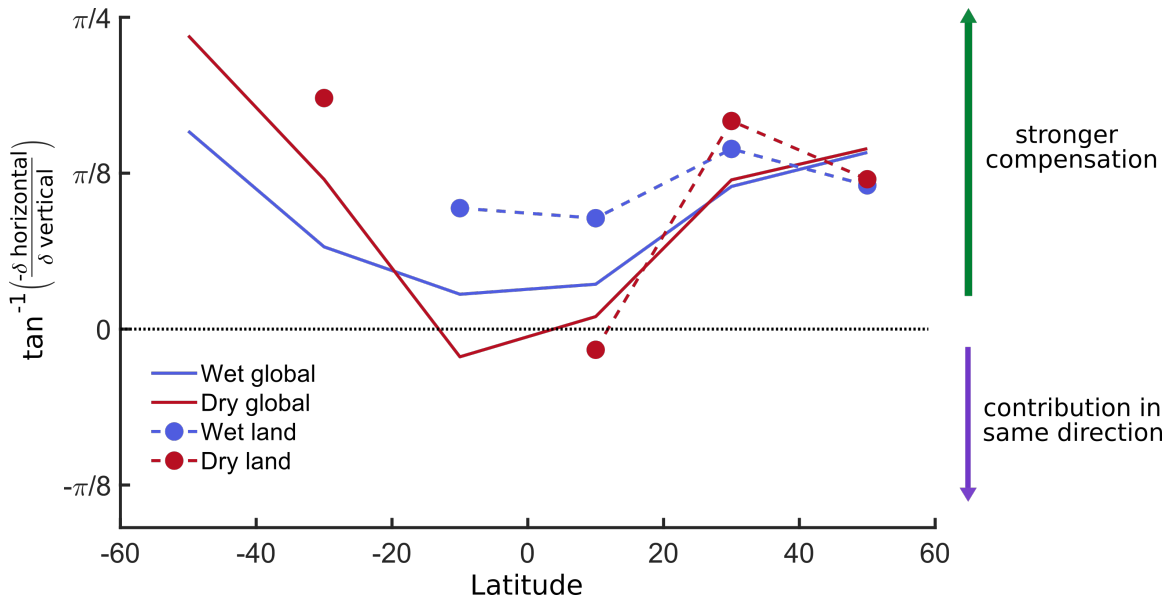


Figure 3-4: Cancellation of the changes in vertical and horizontal advection based on latitude, where a higher positive cancellation implies a closer to full cancellation between the vertical and horizontal advection terms. Negative cancellation means vertical and horizontal advection have the same sign and contribute in the same direction. Spatial averages are taken over either wet or dry regions, but split into 20° latitude bands. Solid lines represent cancellation over the 30% wettest and driest regions of both land and ocean between 60 °S and 60 °N. Dashed lines represent the 30% wettest and driest land regions between 60 °S and 60 °N. Latitude bands with less than 100 valid gridpoints are excluded due to noise (i.e. land in the Southern Hemisphere).

terms will tend to cancel. They find that in the tropics, vertical advection will dominate in transporting excess heating, while at higher latitudes, horizontal advection becomes more important, resulting in greater cancellation at higher latitudes than in the tropics (Hoskins & Karoly, 1981).

The latitudinal dependence of the cancellation between the change in vertical and horizontal advection is plotted in Figure 3-4. Wet and dry regions for these analyses were calculated as described in section 2.4, but using 1) all land and ocean regions between 60 °S and 60 N and 2) all land regions between 60 °S and 60 N. Each wet or dry region was then split into 20-degree latitude bands and spatial averages were taken over each latitude band. Wet or dry regions in which fewer than 100 gridpoints existed within a latitude band were excluded to reduce noise due to random variability. Cancellation is taken to be  $\tan^{-1}(\frac{-\delta H_{x,y}}{\delta H_z})$ . Complete cancellation between advection

terms is when the ratio of  $\frac{\delta H_{x,y}}{\delta H_z}$  is -1 resulting in a cancellation parameter of  $\pi/4$ . Cancellation below 0 means both vertical and horizontal advection contribute towards changes in precipitation in the same direction.

In global wet and dry regions, there is a trend of increased cancellation with latitude, with smaller cancellation in the tropics. Latitude bands that had sufficient wet or dry land gridpoints follow a similar pattern. Cancellation is higher over tropical land regions than over land and ocean, which aligns with the energy budget in Figure 3-1, though these plots cannot be directly compared since the wet and dry regions over tropical land and over land overall are not identical. There does not seem to be a clear difference in cancellation between wet and dry regions.

The strong cancellation between advection terms in the midlatitudes helps explain why the advective terms are relatively unimportant in setting the magnitude of precipitation change over wet and dry land regions, despite the strong spatial pattern in Figure 2-1. In the midlatitudes, the advection terms nearly completely cancel each other out. In the tropics, horizontal advection is very weak, while vertical advection has its own internal cancellation between the dynamic and thermodynamic components. This leaves radiative and sensible heat fluxes to set the magnitude and sign of changes in precipitation.

# Chapter 4

## Further interpretations of the tropical energy budget

### 4.1 Shifting wet and dry regions

The wet and dry regions used for all above analyses were computed using an average of annual precipitation over both the historical and future periods. If wet and dry regions move with climate change, then changes in precipitation could be simply due to a wet region moving into the boundary of a previously dry region (and vice versa). This approach also does not account for seasonal differences in precipitation, such as monsoons or tropical regions with wet and dry seasons. Following the approach of Polson and Hegerl (2017), we explore how allowing wet and dry regions to change based on time period or season affects the regionally-averaged energy budget.

The regionally-averaged change in precipitation is plotted in Figure 4-1, allowing regions to change between time periods and/or seasons. To create regions that shift over time period, we create two sets of wet and dry regions, one for the historical period (1980-1999) and one for the climate change period (2081-2100). Regional averages are then taken over these two sets of wet and dry regions for each period separately before calculating the change between the two periods. Seasonally-shifting regions are created similarly; wet and dry regions are calculated using the average precipitation of each individual season, and regional averages for each season are

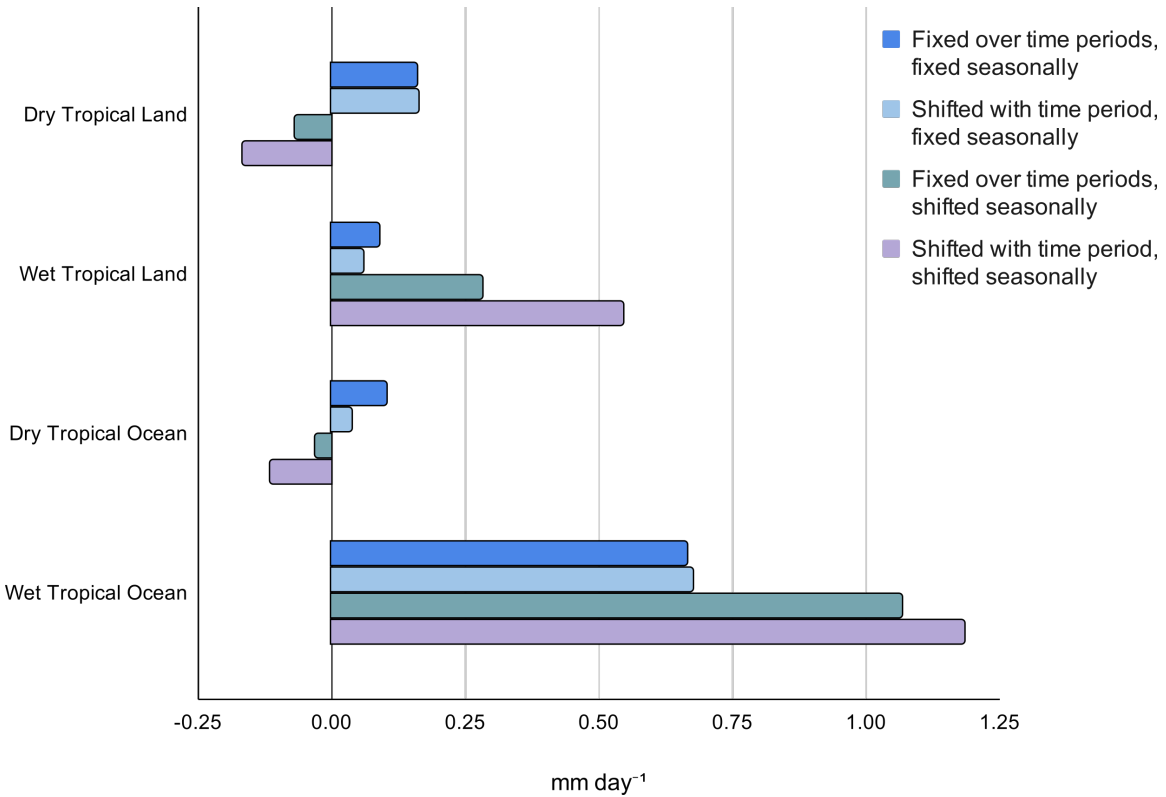


Figure 4-1: Change in precipitation over both fixed and shifted wet and dry tropical regions. Seasonally-shifted regions are calculated based on average precipitation for each individual season, while regions that shift with time period are calculated based on average precipitation for either the historical (1980-1999) or future (2081-2100) time periods.

computed before averaging over the full year.

Allowing for regions to shift only across time period still opposes WWDD, but seasonally shifting regions results in a decrease in precipitation in dry regions and a stronger increase in precipitation in wet regions. The seasonally-shifted result aligns with previous work showing the increasing contrast between wet and dry seasons (Chou et al., 2013). If regions are chosen to follow the wettest and driest gridpoints for each season, the dynamical effects from regions of strong ascent or descent moving based on an annual cycle are reduced, and the thermodynamic mechanism can dominate, driving WWDD. Thus, in the seasonally-shifted case, we would expect to see a strongly negative change in vertical advection in dry regions and with the opposite in wet regions. However, this finding suggests that movement of regions with climate change do not fully explain the dynamic component of vertical advection opposing the WWDD mechanism in the annual average, and a general weakening of the circulation may still be part of the story.

The same regionally-averaged energy budget as Figure 3-1 but with regions that are allowed to change based on season is plotted in Figure 4-2. We use seasonally-shifted regions rather than regions that shift with time period because many tropical land regions currently see strong differences in precipitation based on wet or dry seasons, and changes in the severity of dry and wet seasons will be important in the future. As described above, the vertical advection term is strongly negative over seasonally-shifted dry tropical land, driving a decrease in precipitation, and flips sign over tropical wet land to drive increased precipitation, following WWDD. Sensible heat flux also has a much stronger negative contribution over dry tropical land, which could relate to the surface energy argument from section 3.2. The driest regions are most likely to be moisture-limited and shift from latent to sensible heat, resulting in a stronger increase in sensible heat (and a corresponding decrease in latent heat and precipitation). However, the residual is larger in both regions when allowing regions to shift seasonally, which means the energy budget does not close, and there could be an error in calculating the energy budget in this way.

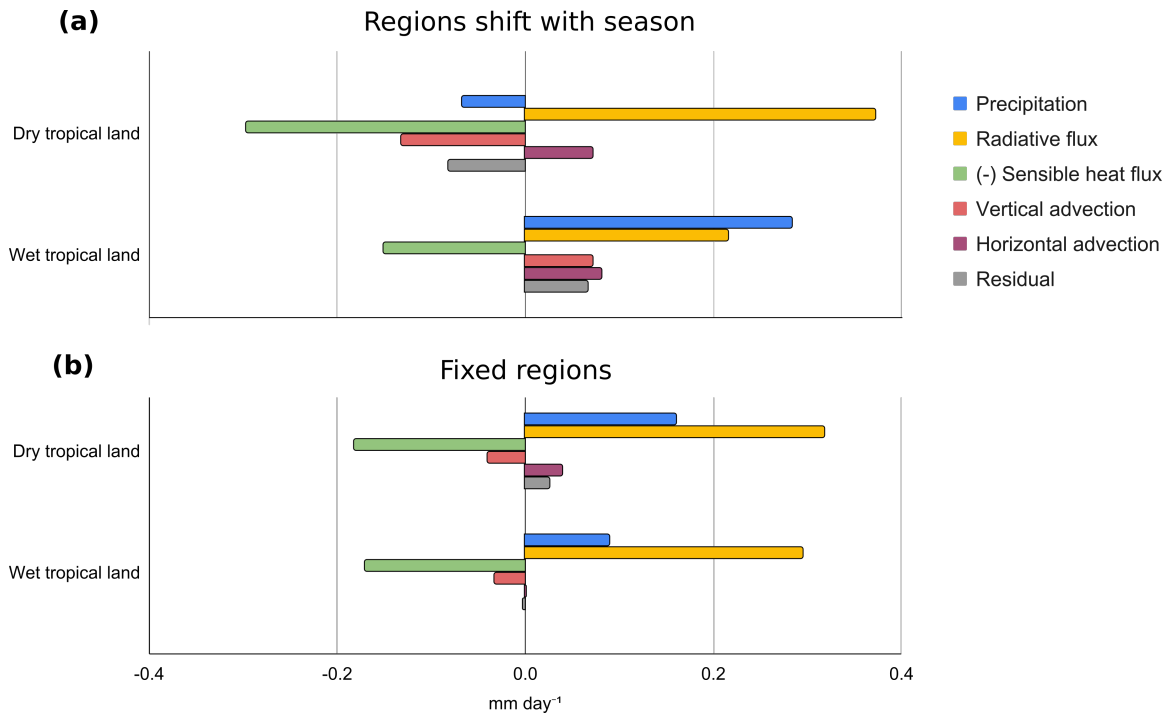


Figure 4-2: Regional averages of changes in each term of the energy budget in  $\text{mm day}^{-1}$ . Top: wet and dry regions are calculated based on average precipitation (over the full 40-yr time period) for each season. Spatial averages are computed for each individual season, and then averaged over the full year. Bottom: same as Figure 3-1, where wet and dry regions remain fixed over the full year and time period.

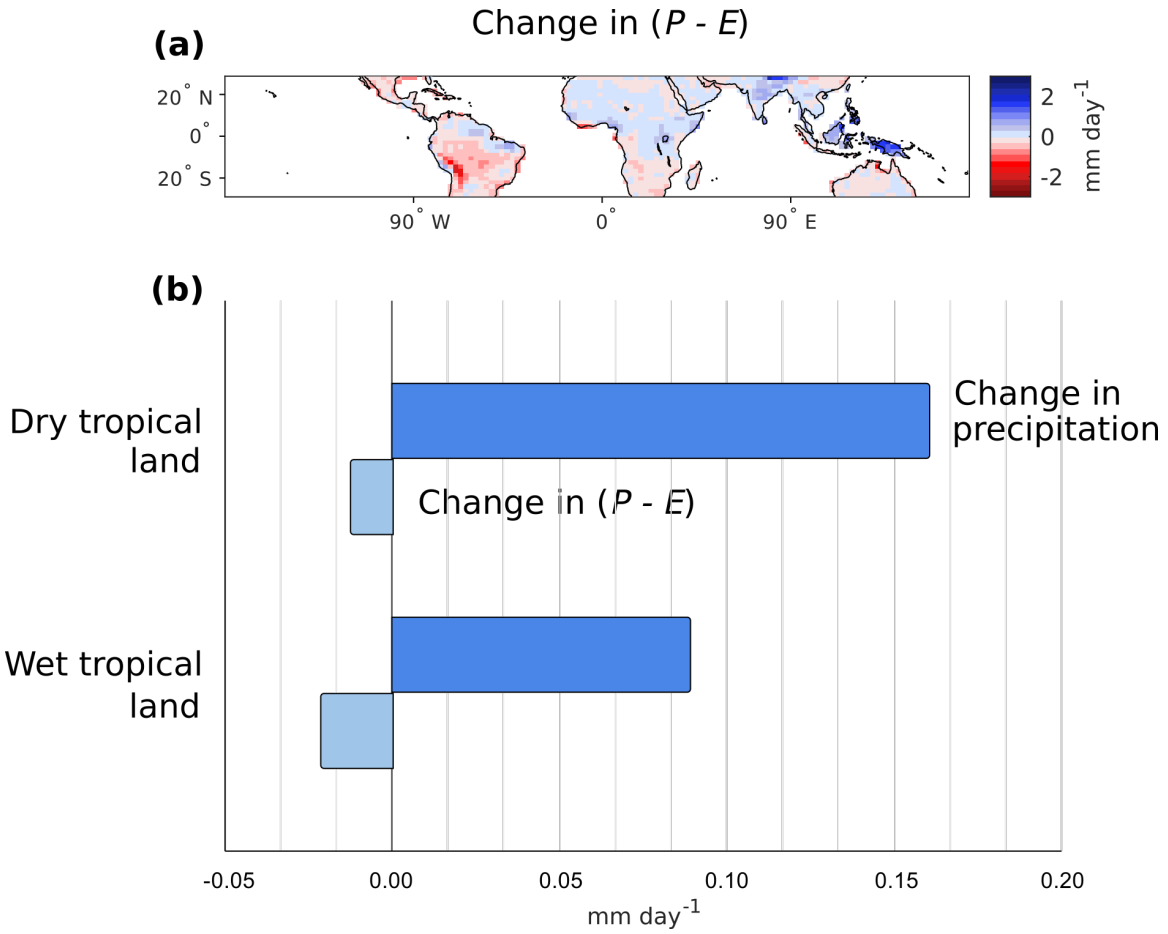


Figure 4-3: (a): Change in  $P - E$  in tropical land regions. (b): Regional averages of changes in precipitation (dark blue) and change in  $P - E$  (light blue) in mm day<sup>-1</sup>.

## 4.2 Precipitation - Evaporation

The energetic framework allows for a simple understanding of changes in precipitation over tropical regions, but many studies focus instead on changes in precipitation minus evaporation ( $P - E$ ) using the water vapor budget. Evaporation can also be considered from an energetic mindset: the energy to drive evaporation is driven by changes in surface energy fluxes: radiative loss and sensible heat flux. An increase in radiative loss will increase evaporation, and with enough moisture availability, evaporation can exceed the increased radiative loss if sensible heat flux directs energy from the atmosphere to the surface (Pierrehumbert, 2002). Thus, evaporation is constrained by the surface energy budget in a similar way to precipitation.

The spatial map and regional averages of  $P - E$  over tropical land is plotted in

Figure 4-3. In many locations and in the regional average, the increase in evaporation exceeds the increase in precipitation, resulting in a decrease in  $P - E$ . An interesting exception is the increase in  $P - E$  over Indonesia and India. As discussed in section 3.2, there is an asymmetry between the wet tropical rainforests of Indonesia and South America in the change in sensible heat flux, which is similar to the asymmetry in the change in  $P - E$ .

The results in section 3 suggest that, on average, most regions will see an increase in precipitation with climate change, but this result may be misleading when considering the change in water availability in these regions. If evaporation increases with or even exceeds precipitation, then regions may see a decrease in available water, all things being equal. There are many situations where an increase in annual average precipitation may not result in an increase in the water available for drinking, agriculture or other human uses; if precipitation mostly falls in extreme precipitation events, water could be lost due to excessive runoff or could evaporate before it can replenish the water table. Thus, understanding the energetics behind changes in precipitation as well as the changes in available water at the surface (i.e. using the water vapor budget) is important to prepare communities for climate change.

# Chapter 5

## Conclusions

The failure of the WWDD mechanism over land becomes more clear when using an energetic approach. In large-scale regional averages over wet and dry tropical land, increases in precipitation are mainly due to an overall increase in net radiation and offset by increases in sensible heat flux. Vertical and horizontal advection, which may be important on smaller, local scales, tend to be very small in the regional mean. The dynamic and thermodynamic components of vertical advection tend to oppose each other, reducing the magnitude of the regionally-averaged vertical advection term, and horizontal advection is generally small in the tropics for dynamical reasons (Hoskins & Karoly, 1981).

The internal cancellation in the vertical advection term becomes quite important, especially when considering that wet and dry regions shift seasonally and may shift with climate change. The thermodynamic component of vertical advection gives the WWDD mechanism, but this effect is opposed by dynamic changes brought on by wet regions moving into dry regions and vice versa with climate change. When wet and dry regions are allowed to shift based on the season, the WWDD mechanism becomes more dominant. An interesting extension of this idea would be to test whether any arbitrary shift of wet and dry regions would inherently oppose WWDD. This would help understand whether the opposition of the dynamic component of vertical advection to WWDD is a factor of how regions are selected or due to some physical mechanism.

The perturbation energy budget approach used in this study is helpful towards understanding the patterns of changes in precipitation over land with climate change, but there are several limitations that could be resolved with future study. All above analyses were performed using one global climate model, but different climate models may have varying climatologies and energetic responses to climate change. Previous studies that have used a multi-model mean have shown high variability of changes in precipitation in dry regions (Donat et al., 2016; Polson & Hegerl, 2017), so the results in this study could vary significantly with a different model. The use of global climate models has its own drawbacks, especially without comparing results to historical observations, since models are not perfectly representative of the real climate system. In particular, models may overestimate weakening circulation patterns, and a lack of widespread observations of land surface variables make land-atmosphere coupling particularly difficult.

Future studies could expand beyond this study by trying to reduce the complexity that arises from using land surface variables. One way to do this would be to use the atmospheric energy budget of the full atmosphere above the level of condensation (LCL), excluding turbulent fluxes directly above the surface, following Takahashi (2009). This approach would reduce the uncertainty of sensible heat fluxes at the surface, but also eliminate noise due to orography in the advective terms. Further, the seasonal dependence of these results could be examined more deeply to better understand the seasonally-shifted results in section 4.1. This work provides groundwork for an understanding of regional tropical precipitation changes over land, but further work will help us better understand the changes that we may see with future climate change.

# Appendix A

## Calculating advection terms using hybrid sigma coordinates

Equation 2.6 shows the vertical and horizontal advection terms in pressure coordinates, but 6-hourly data is provided in hybrid sigma coordinates. At the lower boundary, the hybrid sigma coordinate is similar to a sigma coordinate, where height is given by pressure divided by surface pressure, but the hybrid sigma coordinate reduces to pressure near the top of the atmosphere. The coordinate is described more formally in Simmons and Burridge (1981).

The GFDL-CM3 model defines the hybrid sigma coordinate where:

$$p = a(\eta)p_0 + b(\eta)p_s \quad (\text{A.1})$$

where  $p_0$  and  $p_s$  are constants representing a reference pressure and surface pressure, respectively, and  $\eta$  represents each vertical level in the model.  $a$  and  $b$  are vertical vectors of scalars that weight the reference and surface pressure at each vertical level.

Integrating the horizontal advection terms requires calculating the horizontal derivative along constant pressure surfaces. Since pressure is a function of the vertical level and surface pressure varies horizontally, an extra term that relates horizontal gradients in surface pressure is required. We calculate this term as follows:

For an arbitrary variable  $A$  taken in the arbitrary horizontal direction  $x$ :

$$\left. \frac{\partial A}{\partial x} \right|_p = \left. \frac{\partial A}{\partial x} \right|_\eta + \left. \frac{\partial A}{\partial \eta} \frac{\partial \eta}{\partial x} \right|_p \quad (\text{A.2})$$

We can evaluate the first term on the right side of equation A.2 using model output. To calculate the second term, we take the derivative at constant pressure using  $p$  in equation A.1:

$$\left. \frac{\partial p}{\partial x} \right|_p = 0 = a' p_0 \left. \frac{\partial \eta}{\partial x} \right|_p + b' p_s \left. \frac{\partial \eta}{\partial x} \right|_p + b \frac{\partial p_s}{\partial x} \quad (\text{A.3})$$

$$\left. \frac{\partial \eta}{\partial x} \right|_p = \frac{-b \frac{\partial p_s}{\partial x}}{a' p_0 + b' p_s} \quad (\text{A.4})$$

The hybrid sigma derivative of  $A$  is:

$$\frac{\partial A}{\partial \eta} = \frac{\partial A}{\partial p} \frac{\partial p}{\partial \eta} = \frac{\partial A}{\partial p} (a' p_0 + b' p_s) \quad (\text{A.5})$$

Substituting A.4 and A.5 into equation A.2 gives

$$\left. \frac{\partial A}{\partial x} \right|_p = \left. \frac{\partial A}{\partial x} \right|_\eta - \frac{b \frac{\partial p_s}{\partial x}}{a' p_0 + b' p_s} \frac{\partial A}{\partial p} (a' p_0 + b' p_s) \quad (\text{A.6})$$

$$\left. \frac{\partial A}{\partial x} \right|_p = \left. \frac{\partial A}{\partial x} \right|_\eta - b \frac{\partial p_s}{\partial x} \frac{\partial A}{\partial p} \quad (\text{A.7})$$

For the horizontal advection term in equation 2.6, copied below:

$$\int_0^{p_s} \left( \frac{u}{a \cos(\phi)} \frac{\partial s}{\partial \lambda} + \frac{v}{a} \frac{\partial s}{\partial \phi} \right) \frac{dp}{g} \quad (\text{A.8})$$

and with the expression for the horizontal derivative of surface pressure in equation A.7, the horizontal advection term becomes:

$$\int_0^{p_s} \left( \frac{u}{a \cos(\phi)} \left. \frac{\partial s}{\partial \lambda} \right|_\eta - b \frac{u}{a \cos(\phi)} \frac{\partial s}{\partial p} \frac{\partial p_s}{\partial \lambda} + \frac{v}{a} \left. \frac{\partial s}{\partial \phi} \right|_\eta - b \frac{v}{a} \frac{\partial s}{\partial p} \frac{\partial p_s}{\partial \phi} \right) \frac{dp}{g} \quad (\text{A.9})$$

Dry static energy involves a geopotential term  $gz$  which can be calculated analyt-

ically using hydrostatic balance:

$$\frac{\partial z}{\partial p} = \frac{-1}{\rho g} \quad (\text{A.10})$$

where  $\rho$  is the density of air. Using the equation of state for air  $p = \rho R T_v$  with  $T_v$  as virtual temperature, which takes into account the relative humidity of the air at each level, we get:

$$\frac{\partial z}{\partial p} = \frac{-R T_v}{p g} \quad (\text{A.11})$$

Equation A.11 can be substituted into both equation A.9 and the equation for vertical advection (equation 2.4) to avoid having to calculate  $z$  separately, which could introduce numerical errors.

## Appendix B

### Extensions to the midlatitudes

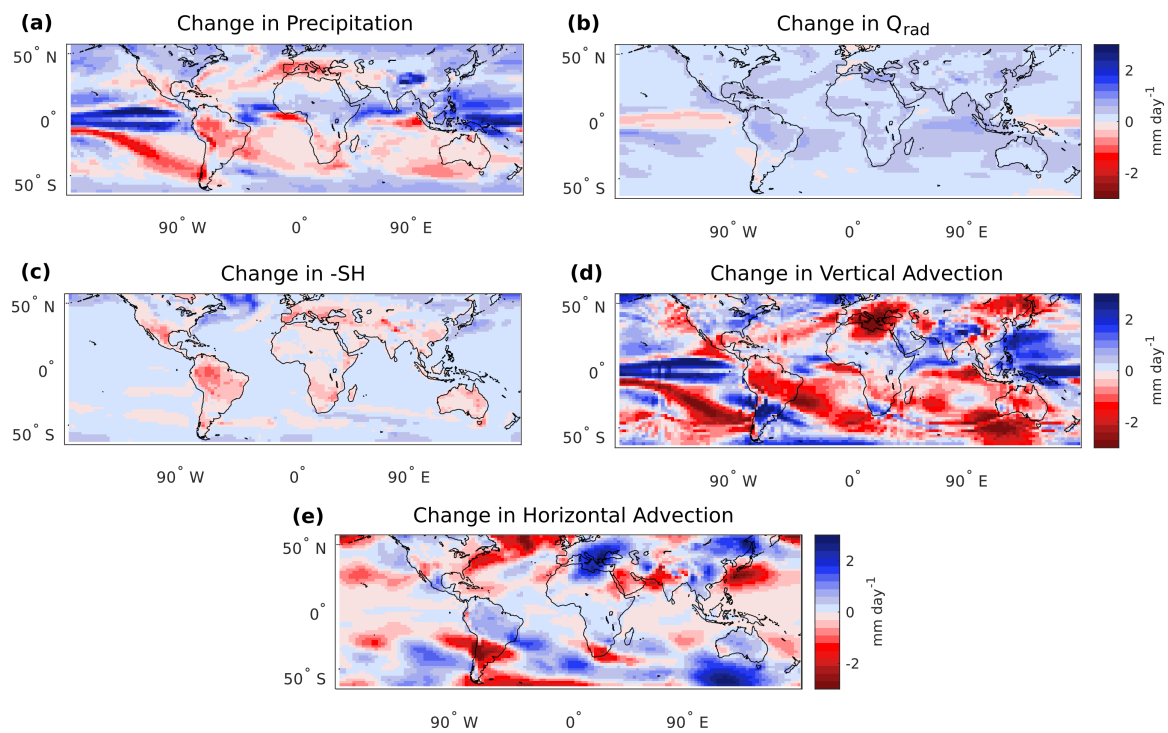


Figure B-1: Same as Figure 2-1, but including land and ocean model output from 60 °S to 60 °N.

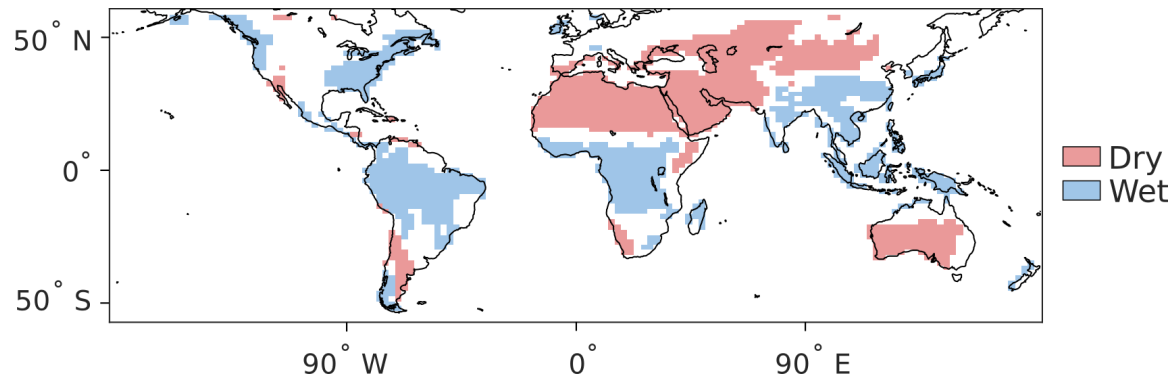


Figure B-2: Same as Figure 2-2, but where wet and dry regions are calculated as the land regions with 30% highest or lowest average annual precipitation, extending from 60 °S to 60 °N.

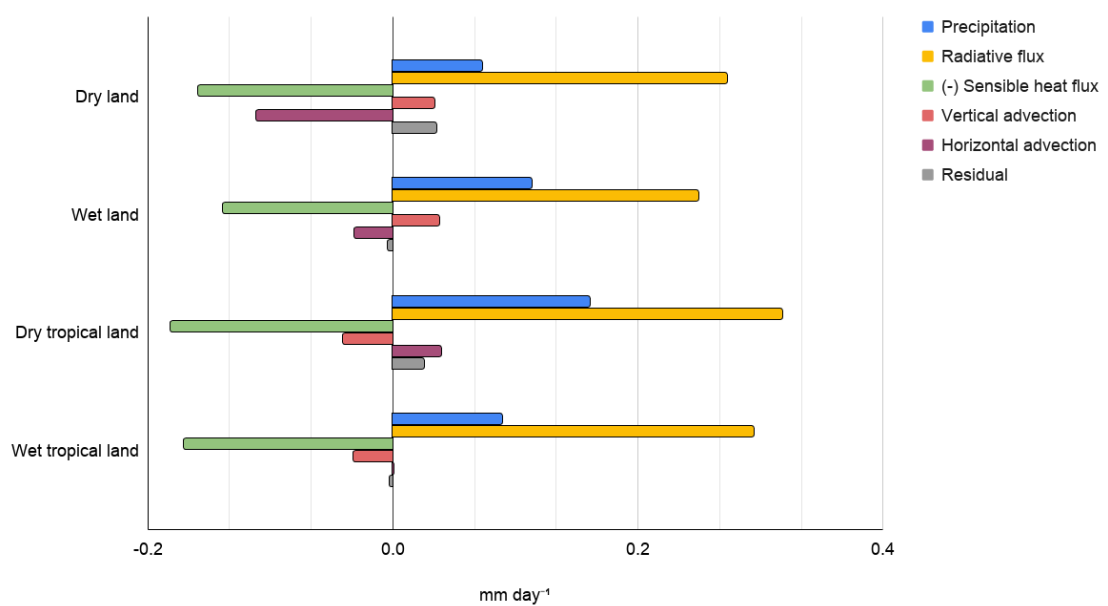


Figure B-3: Same as Figure 3-1 but with spatial averages over dry and wet land for all land ( $60^{\circ}\text{S}$  to  $60^{\circ}\text{N}$ ) and tropical land.

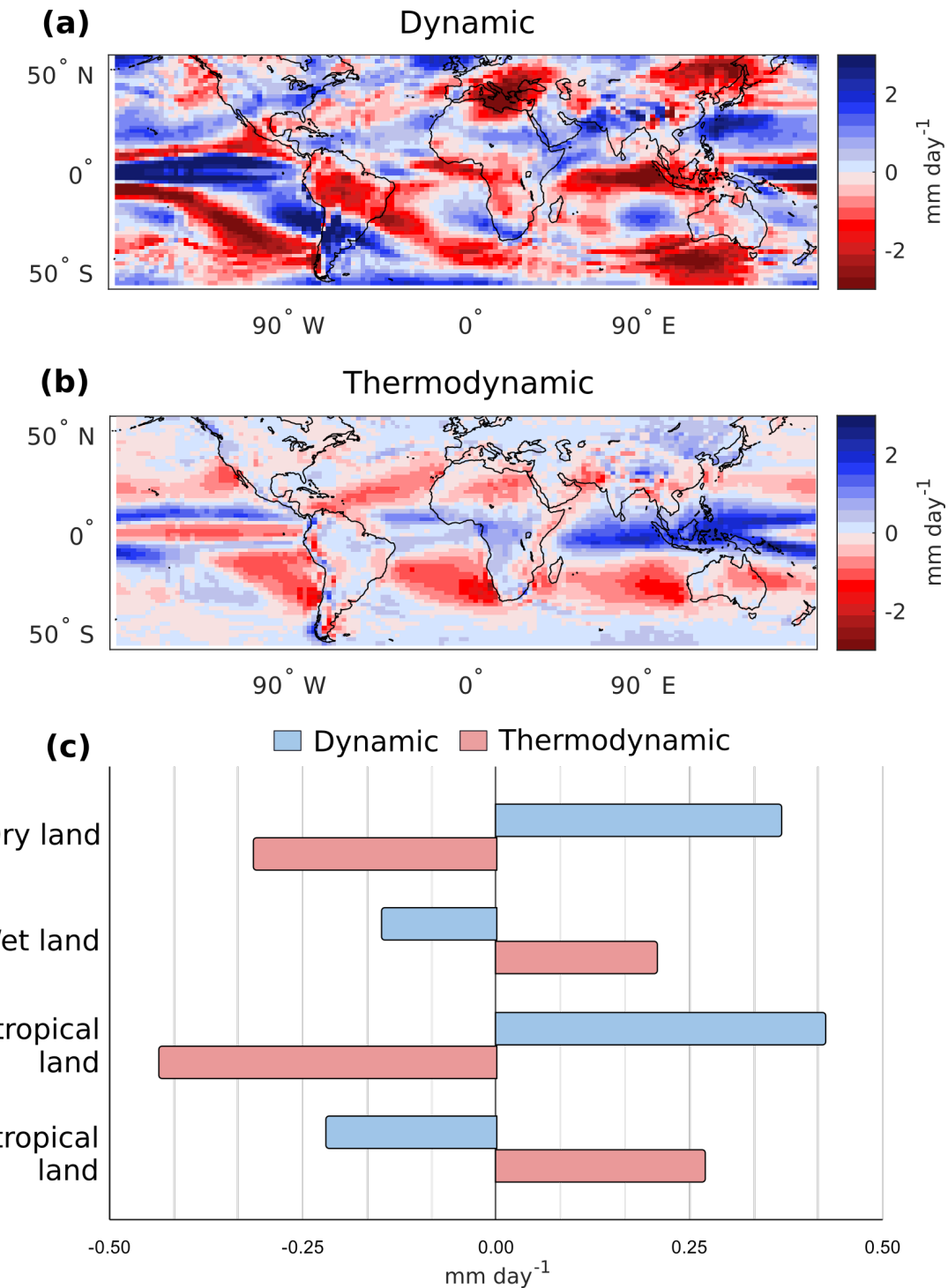


Figure B-4: Same as Figure 3-2, but (a) and (b) include land and ocean model output from 60 °S to 60 °N; and (c) includes spatial averages over dry and wet land regions from 60 °S to 60 °N.

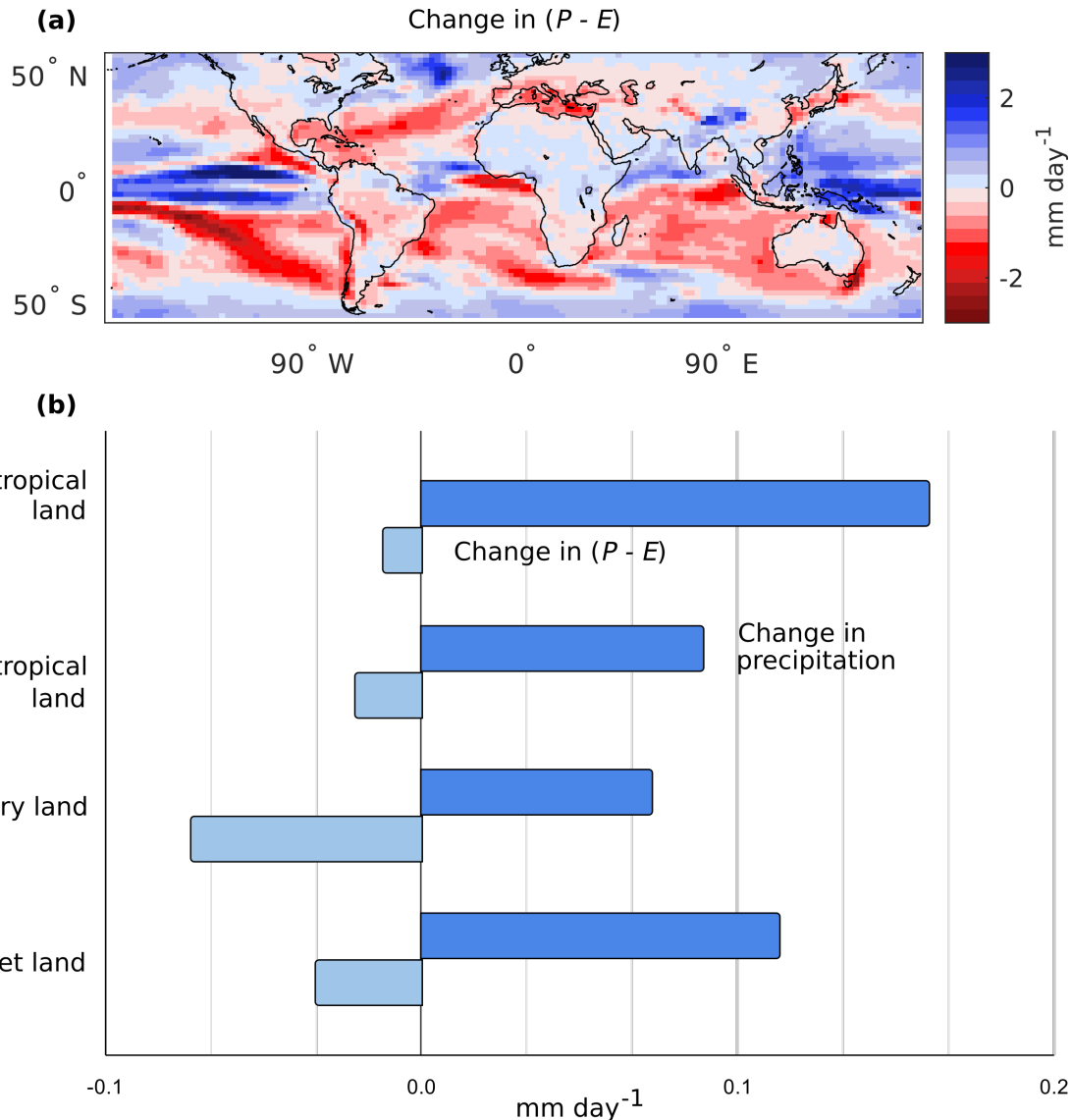


Figure B-5: Same as Figure 4-3, but (a) includes land and ocean model output from 60 °S to 60 °N and (b) includes spatial averages over dry and wet land regions from 60 °S to 60 °N.

# References

- Allen, M. R., & Ingram, W. J. (2002). Constraints on future changes in climate and the hydrologic cycle. *Nature*, 419, 228-232. doi: <https://doi.org/10.1038/nature01092>
- Byrne, M. P., & O'Gorman, P. A. (2015). The response of precipitation minus evapotranspiration to climate warming: Why the “wet-get-wetter, dry-get-drier” scaling does not hold over land. *Journal of Climate*, 28(20), 8078 - 8092. doi: 10.1175/JCLI-D-15-0369.1
- Chadwick, R., Boutle, I., & Martin, G. (2013). Spatial patterns of precipitation change in CMIP5: Why the rich do not get richer in the tropics. *Journal of Climate*, 26(11), 3803 - 3822. doi: 10.1175/JCLI-D-12-00543.1
- Chou, C., Chiang, J. C. H., Lan, C.-W., Chung, C.-H., Liao, Y.-C., & Lee, C.-J. (2013). Increase in the range between wet and dry season precipitation. *Nature Geoscience*, 6, 263-267. doi: <https://doi.org/10.1038/ngeo1744>
- Chou, C., & Neelin, J. D. (2004). Mechanisms of global warming impacts on regional tropical precipitation. *Journal of Climate*, 17(13), 2688 - 2701. doi: 10.1175/1520-0442(2004)017<2688:MOGWIO>2.0.CO;2
- Delworth, T. L., Broccoli, A. J., Rosati, A., Stouffer, R. J., Balaji, V., Beesley, J. A., ... Zhang, R. (2006). GFDL's CM2 global coupled climate models. Part I: Formulation and simulation characteristics. *Journal of Climate*, 19(5), 643 - 674. doi: 10.1175/JCLI3629.1
- Donat, M. G., Lowry, A. L., Alexander, L. V., O'Gorman, P. A., & Maher, N. (2016). More extreme precipitation in the world's dry and wet regions. *Nature Climate Change*, 6, 508–513. doi: <https://doi.org/10.1038/nclimate2941>
- Donner, L. J., Wyman, B. L., Hemler, R. S., Horowitz, L. W., Ming, Y., Zhao, M., ... Zeng, F. (2011). The dynamical core, physical parameterizations, and basic simulation characteristics of the atmospheric component AM3 of the GFDL global coupled model CM3. *Journal of Climate*, 24(13), 3484 - 3519. doi: 10.1175/2011JCLI3955.1
- Greve, P., Orlowsky, B., Mueller, B., Sheffield, J., Reichstein, M., & Seneviratne, S. (2014). Global assessment of trends in wetting and drying over land. *Nature Geoscience*, 7, 716-721. doi: <https://doi.org/10.1038/ngeo2247>
- Greve, P., & Seneviratne, S. I. (2015). Assessment of future changes in water availability and aridity. *Geophysical Research Letters*, 42(13), 5493-5499. doi: <https://doi.org/10.1002/2015GL064127>
- He, J., & Soden, B. J. (2015). Anthropogenic weakening of the tropical circulation:

- The relative roles of direct CO<sub>2</sub> forcing and sea surface temperature change. *Journal of Climate*, 28(22), 8728 - 8742. doi: 10.1175/JCLI-D-15-0205.1
- Held, I. M., & Soden, B. J. (2006). Robust responses of the hydrological cycle to global warming. *Journal of Climate*, 19(21), 5686 - 5699. doi: 10.1175/JCLI3990.1
- Hoskins, B. J., & Karoly, D. J. (1981). The steady linear response of a spherical atmosphere to thermal and orographic forcing. *Journal of Atmospheric Sciences*, 38(6), 1179 - 1196. doi: 10.1175/1520-0469(1981)038<1179:TSLROA>2.0.CO; 2
- Kooperman, G. J., Chen, Y., Hoffman, F. M., Koven, C. D., Lindsay, K., Pritchard, M. S., ... Randerson, J. T. (2018). Forest response to rising CO<sub>2</sub> drives zonally asymmetric rainfall change over tropical land. *Nature Climate Change*, 8, 434-440. doi: <https://doi.org/10.1038/s41558-018-0144-7>
- Liu, C., & Allan, R. P. (2013). Observed and simulated precipitation responses in wet and dry regions 1850–2100. *Environmental Research Letters*, 8(3). doi: <https://doi.org/10.1088/1748-9326/8/3/034002>
- Lorenz, D. J., & DeWeaver, E. T. (2007). Tropopause height and zonal wind response to global warming in the IPCC scenario integrations. *Journal of Geophysical Research: Atmospheres*, 112(D10). doi: <https://doi.org/10.1029/2006JD008087>
- Ma, J., Xie, S.-P., & Kosaka, Y. (2012). Mechanisms for tropical tropospheric circulation change in response to global warming. *Journal of Climate*, 25(8), 2979 - 2994. doi: 10.1175/JCLI-D-11-00048.1
- Marshall, J., & Plumb, R. A. (2007, December). Atmosphere, ocean, and climate dynamics: An introductory text. In (1st ed., Vol. 93). Amsterdam: Academic Press.
- McColl, K. A., Salvucci, G. D., & Gentine, P. (2019). Surface flux equilibrium theory explains an empirical estimate of water-limited daily evapotranspiration. *Journal of Advances in Modeling Earth Systems*, 11(7), 2036-2049.
- Monteith, J. L. (1965). Evaporation and the environment. *Symposia of the Society for Experimental Biology*, 19, 205-234.
- Morice, C. P., Kennedy, J. J., Rayner, N. A., Winn, J. P., Hogan, E., Killick, R. E., ... Simpson, I. R. (2021). An updated assessment of near-surface temperature change from 1850: The HadCRUT5 data set. *Journal of Geophysical Research: Atmospheres*, 126(3), e2019JD032361. (e2019JD032361 2019JD032361) doi: <https://doi.org/10.1029/2019JD032361>
- Moss, R., Babiker, W., Brinkman, S., Calvo, E., Carter, T., Edmonds, J., ... Zurek, M. (2008). *Towards new scenarios for the analysis of emissions: Climate change, impacts and response strategies*. Geneva, Switzerland: Intergovernmental Panel on Climate Change Secretariat (IPCC). (IPCC Expert Meeting report, 19-21 September, 2007, Noordwijkerhout, The Netherlands : technical summary)
- Muller, C. J., & O'Gorman, P. A. (2011). An energetic perspective on the regional response of precipitation to climate change. *Nature Climate Change*, 1, 266-271. doi: <https://doi.org/10.1038/nclimate1169>
- O'Gorman, P. A., Allen, R. P., Byrne, M. P., & Previdi, M. (2012). Energetic constraints on precipitation under climate change. *Surveys in Geophysics*, 33,

- 585-608. doi: <https://doi.org/10.1007/s10712-011-9159-6>
- Pachauri, R., & Meyer, L. (Eds.). (2014). *Climate change 2014: Synthesis report. contribution of working groups I, II and III to the Fifth Assessment Report of the Intergovernmental Panel on Climate Change.*
- Peixoto, J. P., & Oort, A. H. (1992, February). Physics of climate. In (1st ed.). New York: AIP-Press.
- Pierrehumbert, R. T. (2002). The hydrologic cycle in deep-time climate problems. *Nature*, 419, 191-198. doi: <https://doi.org/10.1038/nature01088>
- Pierrehumbert, R. T. (2010). Principles of planetary climate. In (p. 386-431). Cambridge, UK: Cambridge University Press.
- Polson, D., & Hegerl, G. C. (2017). Strengthening contrast between precipitation in tropical wet and dry regions. *Geophysical Research Letters*, 44(1), 365-373.
- Roderick, M. L., Sun, F., Lim, W. H., & Farquhar, G. D. (2014). A general framework for understanding the response of the water cycle to global warming over land and ocean. *Hydrology and Earth System Sciences*, 18(5), 1575–1589. doi: 10.5194/hess-18-1575-2014
- Schneider, T., O’Gorman, P. A., & Levine, X. J. (2010). Water vapor and the dynamics of climate changes. *Reviews of Geophysics*, 48(3). doi: <https://doi.org/10.1029/2009RG000302>
- Seager, R., Naik, N., & Vecchi, G. A. (2010). Thermodynamic and dynamic mechanisms for large-scale changes in the hydrological cycle in response to global warming. *Journal of Climate*, 23(17), 4651 - 4668. doi: 10.1175/2010JCLI3655.1
- Simmons, A. J., & Burridge, D. M. (1981). An energy and angular-momentum conserving vertical finite-difference scheme and hybrid vertical coordinates. *Monthly Weather Review*, 109(4), 758 - 766. doi: 10.1175/1520-0493(1981)109<0758:AEAAMC>2.0.CO;2
- Singh, M. S., & O’Gorman, P. A. (2012). Upward shift of the atmospheric general circulation under global warming: Theory and simulations. *Journal of Climate*, 25(23), 8259 - 8276. doi: 10.1175/JCLI-D-11-00699.1
- Sohn, B.-J., Lee, S., Chung, E.-S., & Song, H.-J. (2016). The role of the dry static stability for the recent change in the pacific walker circulation. *Journal of Climate*, 29(8), 2765 - 2779. doi: 10.1175/JCLI-D-15-0374.1
- Takahashi, K. (2009). The global hydrological cycle and atmospheric shortwave absorption in climate models under CO<sub>2</sub> forcing. *Journal of Climate*, 22(21), 5667 - 5675. doi: 10.1175/2009JCLI2674.1
- Trenberth, K. E., & Guillemot, C. J. (1995). Evaluation of the global atmospheric moisture budget as seen from analyses. *Journal of Climate*, 8(9), 2255 - 2272. doi: 10.1175/1520-0442(1995)008<2255:EOTGAM>2.0.CO;2
- Vecchi, G. A., & Soden, B. J. (2007). Global warming and the weakening of the tropical circulation. *Journal of Climate*, 20(17), 4316 - 4340. doi: 10.1175/JCLI4258.1
- Zarakas, C. M., Swann, A. L. S., Laguë, M. M., Armour, K. C., & Randerson, J. T. (2020). Plant physiology increases the magnitude and spread of the transient

- climate response to CO<sub>2</sub> in CMIP6 earth system models. *Journal of Climate*, 33(19), 8561 - 8578. doi: 10.1175/JCLI-D-20-0078.1
- Zarch, M. A. A., Sivakumar, B., & Sharma, A. (2015). Assessment of global aridity change. *Journal of Hydrology*, 520, 300-313. doi: <https://doi.org/10.1016/j.jhydrol.2014.11.033>